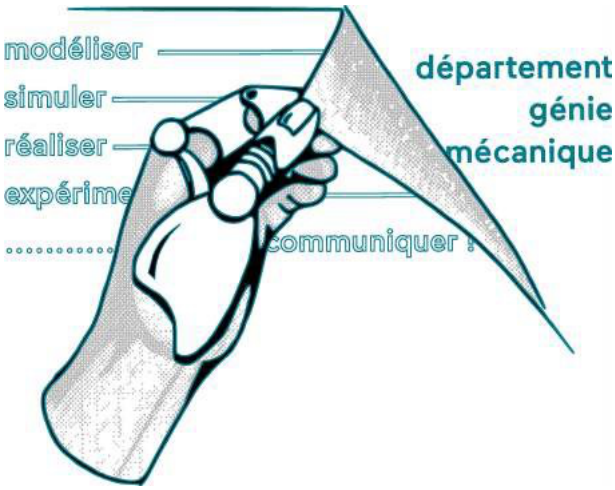

RESEARCH PROJECTS

STUDENTS OF THE DEPARTMENT OF MECHANICAL ENGINEERING

2023-2024

ABSTRACT

Structure of human collagen fiber organization in connective tissues

Guidelines for authors

S. BAALACHE - S. BOUICHER - E.BUDYN

TER M1 2023-2024

FINAL DEFENCE OF RESEARCH PROJECTS

April 2, 2024, Gif-sur-Yvette, France

école normale supérieure paris–saclay

TER M1 2023-2024
FINAL DEFENCE OF RESEARCH PROJECTS
April 2, 2024, Gif-sur-Yvette, France

Structure of human collagen fiber organization in connective tissues Guidelines for authors

S. Baalache*, S. Bouicher†, E.Budyn◇

Department of Mechanical Engineering
Ecole Normale Supérieure Paris-Saclay, University Paris-Saclay
4 av des Sciences 91190, Gif-Sur-Yvette
*e-mail: selma.baalache@ens-paris-saclay.fr
† e-mail: segan.bouicher@ens-paris-saclay.fr
◇ e-mail: elisa.budyn@ens-paris-saclay.fr

KEYWORDS: Cortical bone; Osteocyte; Collagen fiber; Composite; Mechanical constitutive law.

ABSTRACT

Introduction

Bone is known to be a mechanostat and adapt its microstructure to the loading it is subjected to. With aging and certain pathologies this adaptation is modified [1]. As a baseline, we propose to identify in healthy bone, the limit of elasticity of the constitutive behaviors of the materials phases present in the micro-environment of an osteocyte.

Materials and Methods

A Representative Volume Element, RVE, of the bone matrix around an osteocyte process was constructed by segmentation of fluorescent confocal microscopy observations [1] of the cell and Transmission Electron Microscopy (TEM) images of the mineralized fibers [2]. The mineralized collagen fibers of the extracellular matrix around the osteocyte cytoplasmic extension was modeled by 3D helicoidal tubular structures parameterized by the TEM measurements. Only dark osteons of which the collagen fibers display a 60°/120° orientation were considered [2]. These osteons usually form in regions that mostly work under tension [3]. Because long bones such as tibia and femur work under flexion, therefore under compression and tension, both types of loading were modeled at the limit strain of homeostasis: 1500 micro-strain under compression and 1000 micro-strain under tension [4]. As a preliminary approximation, all the materials phases including the hydroxyapatite (HAP), Type I collagen, the proteoglycan interphase, the peri-cellular matrix (PCM), and the cell process were considered linear elastic. The finite element model was implemented in Abaqus. The obtained principal components of the stress fields of the different phases were projected on a unit sphere to identify directional behaviors and limits of elasticity.

Results and discussions

Under 1500 compressive micro-strain of the RVE, the hydroxyapatite phase displays significantly higher compressive stress values than other phases. The cell process is under a

minimal principal stress of -15 to -40 Pa compression and a maximum principal stress in mixed mode of 10 Pa tension and -10 Pa compression. Under 1000 tensile micro-strain of the RVE, the hydroxyapatite phase displays tensile stress values higher than other phases but most of the phase are under tension with an homogeneous distribution. The cell process is under a minimal principal stress of 5 to 15 Pa tension and a maximum principal stress in mixed mode of 3 Pa tension and -3 Pa compression.

Our model showed in the RVE under $1000\mu\epsilon$ tension, the maximum tensile stress values in the HAP corresponds to the damage threshold at the nano-scale identified by an dual experimental-numerical approach [5]. Moreover, the model showed that fiber orientation generate a stress distribution that is more adequate to either tensile or compressive loading.

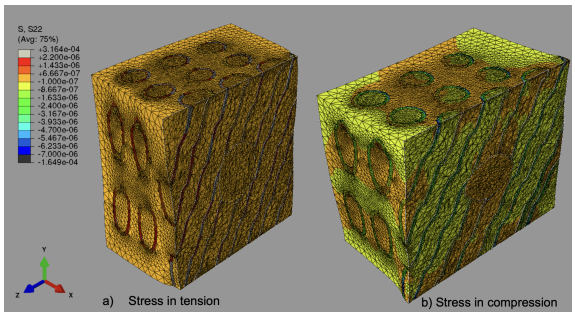

Figure 1: σ_{22} Cauchy stress component in the RVE either (a) under $1\mu\epsilon$ tension or (b) under $1.5\mu\epsilon$ compression.

REFERENCES

[1] E. Budyn. A Bone-on-Chip as a 3D in Vitro Platform to assess the Effect of Stem Cell Age on Tissue Quality and Test Medicines. *Tissue Engineering: Parts A, B, and C.* **Vol**:29 13-14, 2023.

[2] N. Reznikov, R. Shahar, S. Weiner, Three-dimensional structure of human lamellar bone: The presence of two different materials and new insights into the hierarchical organization, Bone. **Vol**:59, 2014

[3] J. Skedros, K. E. Keenan, T. J. Williams, C. J. Kiser, Secondary osteon size and collagen/lamellar organization ("osteon morphotypes") are not coupled, but potentially adapt independently for local strain mode or magnitude, J. Struct. Biol. **Vol**:181 95-107, 2013

[4] R. Al Nazer, J. Lanovaz, C. Kawalilak, J.D. Johnston, S. Kontulainen. Direct in vivo strain measurements in human bone—A systematic literature review. *Journal of Biomechanics* **Vol**:45 27-40, 2011.

[5] J. Jonvaux, T. Hoc, É. Budyn. Analysis of micro fracture in human Haversian cortical bone under compression. *Int. J. Numer. Meth. Biomed. Engng.* **Vol**:28 974-998, September 2012.

Extensional Flow in Dense Suspensions

CHEVRIER Tanguy - GALAS Sébastien - SEGUIN Antoine

TER M1 2023-2024

FINAL DEFENCE OF RESEARCH PROJECTS

April 2, 2024, Gif-sur-Yvette, France

école normale supérieure paris–saclay

Extensional Flow in Dense Suspensions

CHEVRIER Tanguy*, GALAS Sebastien*, SEGUIN Antoine◇

* Mechanical engineering department
Ecole Normale Superieure Paris Saclay
4 avenue des Sciences, 91190 Gif-Sur-Yvette, France
e-mail: tanguy.chevrier@ens-paris-saclay.fr
e-mail: sebastien.galas@ens-paris-saclay.fr

◇ Fluids Automatics and Thermal Systems Laboratory
Batiment Pascal (Bat. 530), Rue André Rivière, 91400 Orsay, France
e-mail: antoine.seguin@universite-paris-saclay.fr

KEYWORDS: dense suspension; extensional flow ; rheological study; image correlation; least-squares matching

ABSTRACT

General Information

The research project focuses on the study of extensional flow in dense suspensions. A suspension is a fluid composed of a liquid phase and a solid phase composed of immersed particles. An extensional or elongational flow simply defines a compressive flow. Extensional flows of dense suspensions are the source of many industrial activities, geophysical phenomena, sanitary processes or new technologies implementing innovative processes.

The rheological study of the flow of dense suspensions began in 1905 with the work of Einstein. Today, the most recent and advanced state of the art was established in 2018 by E. Guazelli and O. Pouliquen [1]. In it, it is established that suspensions can be considered as Newtonian fluids whose viscosity depends on the packing fraction of the suspension and the viscosity of the fluid. The experiment implementing this model was a simple shear flow. Furthermore, the viscosity of a Newtonian fluid is a homogeneous and isotropic characteristic. The viscosity of a suspension should therefore retain these characteristics, given the previous model. So, whatever the geometry and type of flow, the behavior of a Newtonian fluid should be recovered. Nevertheless, related experiments have shown changes in this behavior when considering different flow types and geometries, as shown by Mrs Rashedi [2].So it may be legitimate to question the model, and compare it with other types of flow.

The aim of the project is therefore to characterize the evolution of the velocity field of a dense suspension in extensional flow and compare it with a Newtonian fluid.

Methods

The methods used to determine the flow characteristics involved experimenting using a thin Hele-Shaw cell filled with a model suspension and mass to impose sufficient stress (see Figure 1). Measurements involved filming the experiment from the front, then processing the data using image correlation software (Davis) to obtain the velocity field. This process produced 10 videos, each containing 100 frames of raw data. From the videos, the flow appeared to be stationary, so a scaled study was possible and even necessary to compare all the images, given the evolution of the size of the zone of interest. The raw data were then reorganized into two 3D structures, containing V_x and V_y respectively for the video. As data from different videos have discretizations that do not match, a clustering method was used to calculate a time average and obtain the velocity profiles.

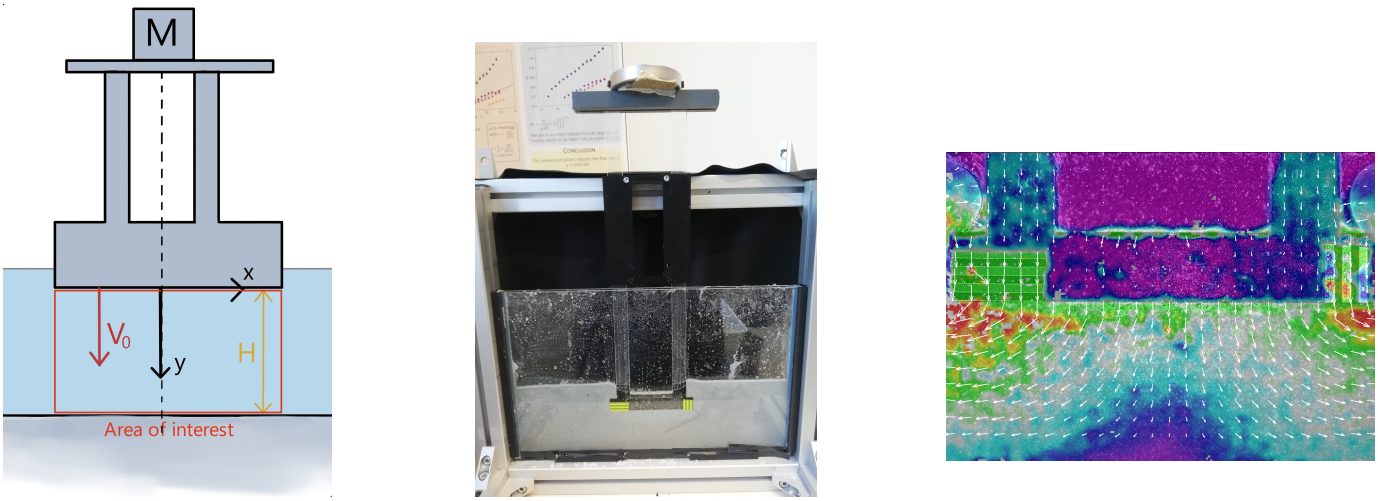

Figure 1: The experimental setup used during the experiments. (left) sketch of the Hele-Shaw cell with displayed x and y axis as well as parameters used for nondimensionalisation such as the speed of the piston for a given frame V_0 and H the height of the area of interest for said frame. (middle) Picture of the Hele-Shaw cell filled with a suspension containing 400 μm PMMA particles with a packing fraction of 46%. The liquid phase is 20% water and 80% glycerol to obtain isodensity. (right) Velocity field calculated by LSM.

Key results and interpretations

The experimental results were compared with an analytical model of a 2D, stationary, incompressible, compressive flow of a Newtonian fluid between two infinite planes (see figure 2).

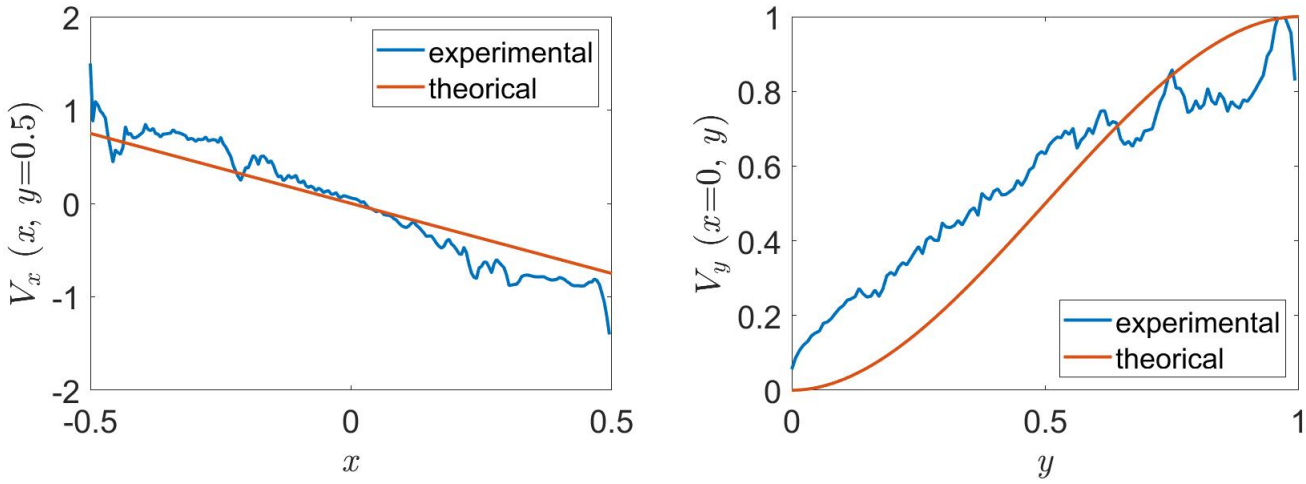

Figure 2: Comparison of experimental (blue) and theoretical (red) velocity fields obtained in significant areas. The V_x velocity profile corresponds fairly well to the analytical field. Nevertheless, the V_y field differs significantly. The similarity in V_x is probably due to the fact that this is the field component with the highest shear.

REFERENCES

[1] Elisabeth Guazzelli, Olivier Pouliquen. Rheology of dense granular suspensions. *Journal of Fluid Mechanics* 852, 2018.

[2] A. Rashedi et al. Shear-induced migration and axial development of particles in channel flows of non-Brownian suspensions. *AIChE Journal* 66:17-100, 2020

Interaction between a gravity driven granular flow and a flexible obstacle

M. FAISY - C. GORAND - Y. BERTHO –
B. DARBOIS-TEXIER - P. GONDRET

TER M1 2023-2024

FINAL DEFENCE OF RESEARCH PROJECTS

April 2, 2024, Gif-sur-Yvette, France

école normale supérieure paris–saclay

TER M1 2023-2024
FINAL DEFENCE OF RESEARCH PROJECTS
April 2, 2024, Gif-sur-Yvette, France

Interaction between a gravity driven granular flow and a flexible obstacle

M. Faisy*, C. Gorand*, Y. Bertho†, B. Darbois-Texier† P. Gondret†

* Département Génie Mécanique, École Normale Supérieure Paris-Saclay
4 Avenue des Sciences 91190 Gif-sur-Yvette
e-mail: matteo.faisy@ens-paris-saclay.fr & clement.gorand@ens-paris-saclay.fr

† Fluides Automatiques et Systèmes Thermiques (FAST), Université Paris-Saclay
Bâtiment Pascal, Rue Andrée Rivière 91400 Orsay
e-mail: {yann.bertho; baptiste.darbois-texier; philippe.gondret}@universite-paris-saclay.fr

KEYWORDS: Granular flow; Fluid-structure interaction ; Continuum Mechanics.

ABSTRACT

General information

Understanding the interactions between a gravity driven granular flow and obstacles could be useful for civil engineering and geophysical applications. Indeed, natural disasters such as landslides or avalanches can occur, and it seems important to look at ways of avoiding or limiting the damages. By observing Nature, it can be seen that it has its own defences against these disasters. The erosion of the dunes is slowed down by a plant called *Ammophila arenaria*, a plant with weak rigidity. A previous study was made looking at the influence of several cylindrical obstacles on a gravity driven granular flow and more particularly how these obstacles can prevent the flow from happening [**1**], but it can be interesting to study flexible obstacles, like in Nature.

Figure 1: Photograph of the flow seen from above

Therefore, the present study experimentally investigates the interaction between a gravity driven granular flow and a singular flexible obstacle, a plastic sheet whose width is 1 cm and height is 5 cm. First, the effect the flow has on the deflection of the object has been observed. Then, the effects the obstacle has on the flow have been explored, such as how the obstacle redirect the current lines, and create stagnation areas (see Figure 1).

Methods

To set up this flow, there was a simple system in which a grain tank was closed by a door whose height could be adjusted, placed on a surface whose inclination could be adjusted as well. At the beginning of the study, to limit the number of parameters, the angle of the plane has been set at 27.5° after finding experimentally that the limit angle at which the flow does not occur is 26°.

To extract data during a flow, a camera was placed just above it, perpendicular to the plane. The height of the flow was measured using a laser line hitting the plane at a sharp angle, and its position on the plane allowed the flow height to be tracked. A video of the flow was then taken and converted into an image sequence. It was analyzed using two *Python* algorithms. While the first one provided spatial measurements of the flow height, the second one established the height of a specific area over time. To measure the object's deflection, images were taken when the flow was judged to be stationary, its height

no longer varying over time. These images were then post-processed on *ImageJ* to locate the object and the free surface (the surface at the height of the flow), enabling the displacement to be measured relative to a reference image.

Results

Following our measurements, the existence of an effect of the flow on the obstacle and vice versa has been demonstrated. By measuring both the flow height and the deflection, it has been shown that the latter depends greatly on the flow height. Two numerical models have been developed and compared to the experimental results. The force of the grains on the object was modelled as an hydrostatic pressure, maximum at the bottom ($z = 0$) and zero at the free surface ($z = H$), written as : $p(z) = \alpha(H - z)$ with H the flow height. After fitting the numerical measurements with the experimental ones, the value of $\alpha = 10.5 \times 10^4$ N.m^{-3} has been determined. Figure 3 displays the displacement at the free surface (δ_H) and at the top of the object (δ_t) measured with three different methods : a Finite Element model using the software *Cast3m*, an analytical model, and the experimental results.

Then, the impact of the object on the flow was analysed. Two distinct zones upstream and downstream of the object can be identified as seen in Figure 1. Downstream, there is a "dead area", with very few grain and very little movements. Upstream, there is a "stagnation area", where the flow height of the flow will increase, in the shape of a triangle. A link between the height far upstream h_∞ and just in front of the obstacle H was investigated, and it was found that there is about a 1.5 ratio between the two.

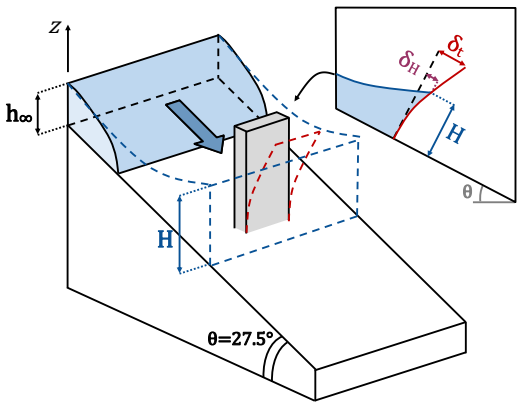

Figure 2: Diagram of the experimental system

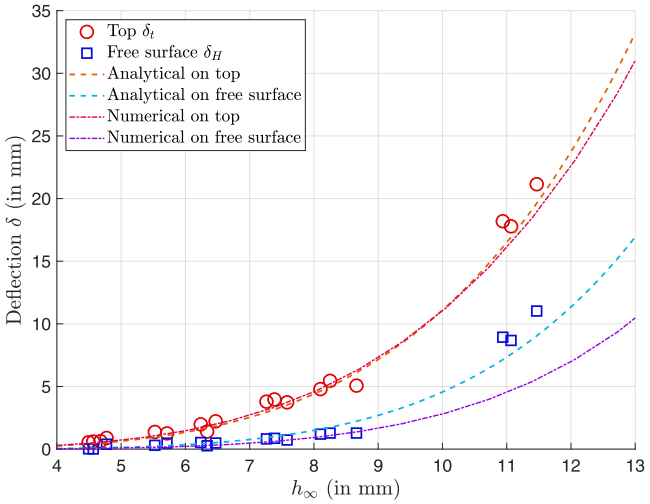

Figure 3: Comparison of the deflection of the free surface and the top of the object for different flow heights, between experimental, analytical and Cast3m results

REFERENCES

[1] Baptiste Darbois Texier, Yann Bertho, Philippe Gondret. *Downslope granular flow through a forest of obstacles* Physical Review Fluids, 2023, 8 (3), pp.034303.

Tomographic monitoring of in-situ tensile test on architectured Aluminium alloy

A. GRAVIL - A. PUJOL - V. KOSIN – B SMANIOTTO - G. TARANTINO – F HILD

TER M1 2023-2024

FINAL DEFENCE OF RESEARCH PROJECTS

April 2, 2024, Gif-sur-Yvette, France

école normale supérieure paris–saclay

Tomographic monitoring of in-situ tensile test on architectured aluminium alloy

A. Gravil,[1] A. Pujol,[1] V. Kosin,[2] B. Smaniotto,[1,2] G. Tarantino,[2] F. Hild[2]

ENS Paris-Saclay 4 avenue des Sciences, 91190 Gif-sur-Yvette, France
e-mail: antoine.pujol@ens-paris-saclay.fr, adrien.gravil@ens-paris-saclay.fr
[1]Department of Mechanical Engineering, [2]LMPS - Laboratoire de Mécanique Paris-Saclay

KEYWORDS: Damage; Digital Volume Correlation; Porous metamaterial; Tomography.

ABSTRACT

Recent advances in additive manufacturing have made it possible to produce porous metamaterials with complex geometries and behavior. The present study deals with a porous metamaterial (Figure 1(a)) whose elliptical pores are topologically generated with a Random Sequential Absorption (RSA) algorithm prior to fabrication using a Laser Powder Bed Fusion (LPBF) process [1]. An earlier study was performed on a similar material but with a circular pore geometry [2]. The aim of this work is to carry out an in-situ tensile test in an X-ray tomograph in order to investigate the interactions between manufacturing defects and geometric porosity.

METHODS

To achieve this main objective, three different steps were carried out. First, an experimental protocol for the in-situ tensile test was defined. It consisted of a sequence of loading and dwell phases. During the loading phases on-the-fly radiographs were collected, while dwell phases corresponded to tomographic scans of the loaded specimen. Around the expected point of fracture, a higher number of scans was acquired (Figure 1(b,c)).

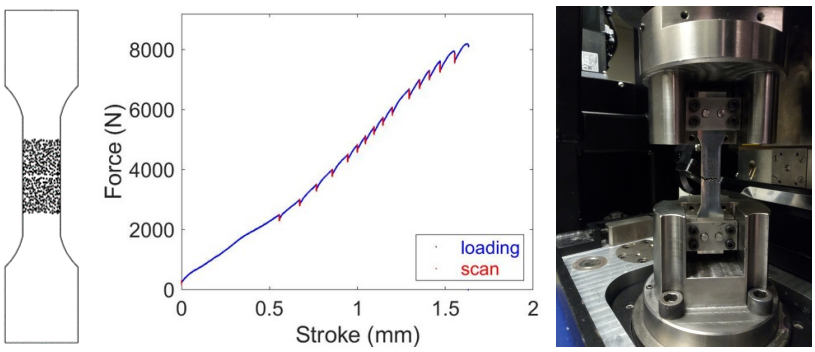

(a) (b) (c)

Figure 1: (a) CAD model of the studied sample. (b) Force-stroke of the in-situ tensile test. (c) Broken sample.

In order to measure displacement fields at any point in the specimen, a global approach of Digital Volume Correlation (DVC) was utilized [3]. A mesh adapted to the actual specimen geometry was created thanks to a backtracking method. To this end, a nominal mesh was first generated using its CAD model and subsequently deformed using the displacement field calculated by DVC. Finally, the final fracture process was analyzed with Projected-based DVC (P-DVC). This method allows the radiographs acquired on the fly to be exploited, and therefore the measurements to be temporally enriched. Specifically, P-DVC was used to study the damage process between the last tomographic scan and fracture as proposed in Ref. [4]. This method is based on the application of Digital Image Correlation (DIC) between a radiograph and a

projection of the deformed volume. The latter is computed from the reference volume, which is deformed by the DVC displacement field multiplied by an unknown amplitude to be determined.

RESULTS

Failure occurred instantaneously at ca. $8.2kN$ without macroscopic softening (Figure 1(b)). This behavior differs from that observed in previous tests carried out on similar mesoporous specimens [2]. The DVC results provided information on the strain and the residual fields. In particular, the gray level residuals were used to identify the crack initiation sites (Figure 2(a)). The latter ones correspond to two manufacturing defects, which are characterized by a local lack of material and are due to the printing strategy. The DVC results were complemented by P-DVC analyses, which provided further insights into the behavior of the specimen up to its final failure. Instantaneous fracture was revealed by a large increase in the P-DVC residuals in the failure zone between the first radiograph acquisition after the last scan and the last one (Figure 2(b,c)). It is thus very likely that, first, the existing manufacturing defect grew under increasing deformation. Then, this crack propagated toward the closest manufacturing defects and eventually traversed the elliptical pores. This crack path was confirmed by observing the first post-mortem radiograph.

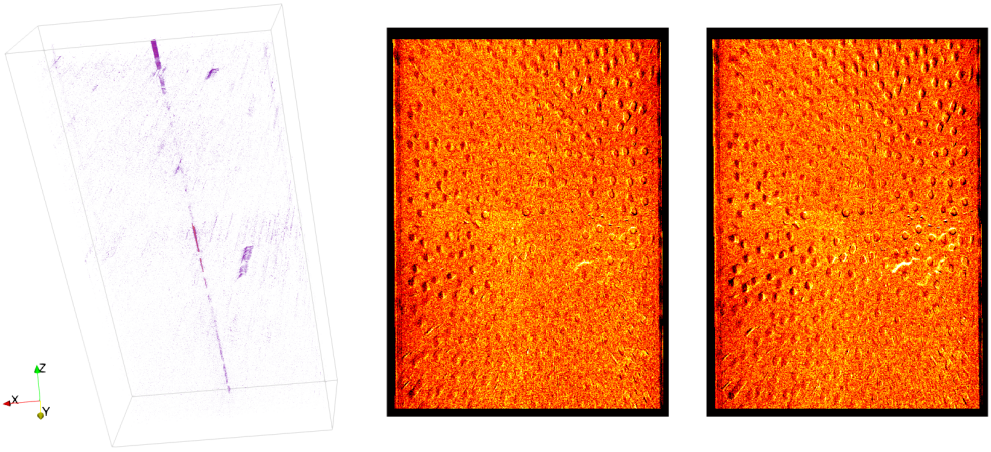

(a) (b) (c)

Figure 2: (a) 3D rendering of thresholded DVC residuals for the last tomographic scan (scan 15). P-DVC residuals for the first radiograph after scan 15 (b) and last radiograph before failure (c).

In summary, the results of this study showed that the manufacturing defects triggered the failure response of the specimen in tension and that the interaction with the mesoporous structure occurred only at the very end of the fracture process. In addition, the use of the P-DVC method enriched the DVC results since it allowed the radiographs acquired on-the-fly to be analyzed up to failure. Overall, the results of this study indicate that manufacturing defects need to taken into account in order to predict the failure behavior of such mesoporous materials.

REFERENCES

[1] CETIM. *Fabrication additive métallique – Les fondamentaux*. Editions Techniques de l'Ingénieur, 2019.

[2] Salvi L. In-situ study of tensile deformation and damage evolution via DIC/DVC of AlSi10Mg cellular materials produced by LPBF. MSc thesis, Politecnico di Milano, 2023.

[3] Roux S et al. Three dimensional image correlation from X-Ray computed tomography of solid foam. *Composites Part A: Applied Science and Manufacturing* 2008; 39(8): 1253–1265.

[4] Kosin V et al. A projection-based approach to extend digital volume correlation for 4D spacetime measurements. *Comptes Rendus Mécanique* 2023; 351: 265–280.

Numerical simulation of a buckling test of honeycomb under bi-compression

Nicolas GUILLOU - Laurent DALMAS de REOTIER

TER M1 2023-2024

FINAL DEFENCE OF RESEARCH PROJECTS

April 2, 2024, Gif-sur-Yvette, France

école normale supérieure paris-saclay

TER M1 2023-2024
FINAL DEFENCE OF RESEARCH PROJECTS
April 2, 2024, Gif-sur-Yvette, France

Numerical simulation of a buckling test of honeycomb under bi-compression

Nicolas Guillou*, Laurent Dalmas de Réotier†

*† Mechanical Engineering Department
Ecole Normale Supérieure Paris-Saclay
4 Avenue des Sciences, 91190 Gif-sur-Yvette
e-mail: *nicolas.guillou@ens-paris-saclay.fr and
†laurent.dalmas_de_reotier@ens-paris-saclay.fr

KEYWORDS: Architectured material, hyperelastic model identification, biaxial compaction

ABSTRACT

General Information

Architectured materials can exhibit enhanced intrinsic properties, such as stiffness anisotropy or specific yield stress, which are not achievable in bulk materials. These exceptional behaviors are due to their cellular structures, composed of slender beams or walls. When subjected to plane loads, these cells tend to buckle as seen on Figure 1.

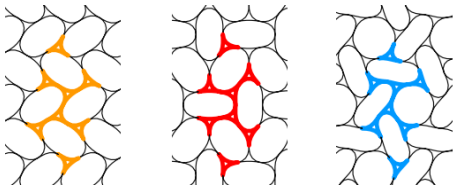

Figure 1: 3 expected buckling modes of a honeycomb [1]

Our project

The objective here is to understand which parameters affect the homogeneity of the buckling of a rubber honeycomb architectured material: the geometry of the specimen, the constitutive material behavior, any manufacturing defects or the boundary conditions. To this aim (1) we conducted mechanical tests on samples to characterize the constitutive material of our honeycomb sample and (2) we used this model to simulate a biaxial compression test of a honeycomb to study its buckling patterns.

Material characterization

We first mold tensile and compression samples using Smooth-Sil 950, a flexible elastomer with high maximum strain. Then, we performed uni-axial tensile and compression tests up to 50% strain and at different speeds to obtain the material behavior. Tension tests were conducted following the ISO 527 norm while compression tests protocol was inspired by the norm [2], we also tried to reduce the impact of friction using lubricant but it inducted out-of-axis displacement and the test failed. Finally, even with high friction, the Poisson's effect seemed to not have an important impact on our measures. We did not observe any effects of the speed on the material behavior in the range of speed studied, so we identified it with a 5-parameters Rivlin model using a fit on both compression and tension curves [3].

The curve obtained with Rivlin model is shown on Figure 2. It fits both tension and compression curves despite the differences of sensors and samples used in the different tests. This responds to the need of characterizing the behavior of the material in tension and in compression to perform numerical simulations of buckling in honeycombs.

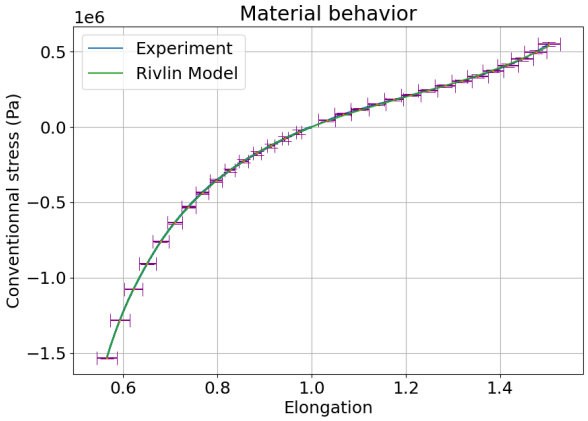

Figure 2: Experimental curve with error bars and Rivlin curve

Finite element simulation

After successfully characterizing our material, the next step was to implement its parameters in our full-field model on LS-Dyna. This finite element software is adapted to our study because it is designed to compute complex phenomenon such as contacts, friction, instabilities and high strain rates. The result is represented on the Figure 3. We observe the intended buckling patterns, however, theoretical results demonstrated [1] that the pattern should be uniform over the surface, which is not the case here. The future objective is to understand why. This numerical tool will be useful to investigate the impact of the material behavior and friction at the boundaries on the sample during the biaxial compression test.

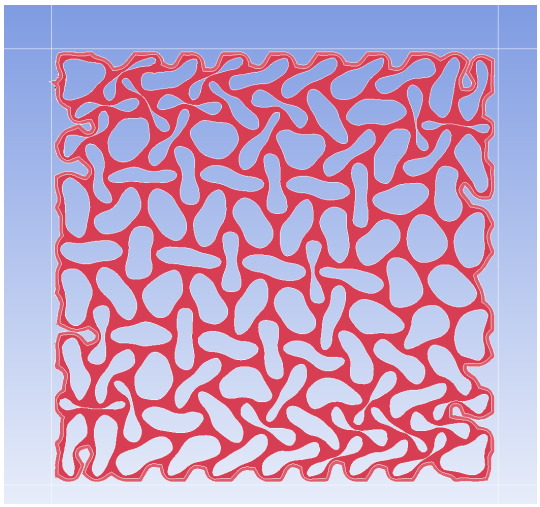

Figure 3: Numerical simulation of a biaxial compression test

REFERENCES

[1] Christelle Combescure, Ryan S. Elliott, Nicolas Triantafyllidis, Deformation patterns and their stability in finitely strained circular cell honeycombs *Journal of the Mechanics and Physics of Solids*, 2020.

[2] AFNOR, Caoutchouc Vulcanisé ou thermoplastique - Détermination des proriétés de contrainte/déformation en comrpession In: *Norme AFNOR*, France, 17 Février 2018

[3] Erwan Verron, Modèles hyperélastiques pour le comportement mécanique des élastomères *Techniques de l'ingénieur*, 2018.

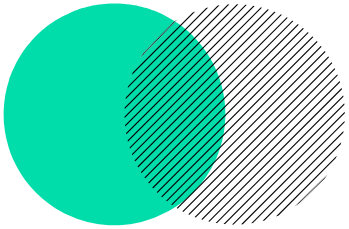

Supervised learning of constitutive laws

B. GAT - O. JEANNE - E.BARANGER

TER M1 2023-2024

FINAL DEFENCE OF RESEARCH PROJECTS

April 2, 2024, Gif-sur-Yvette, France

école normale supérieure paris–saclay

TER M1 2023-2024
FINAL DEFENCE OF RESEARCH PROJECTS
April 2, 2024, Gif-sur-Yvette, France

Supervised learning of constitutive laws

B. Gat*, O. Jeanne†, E. Baranger◊

*†◊ Mechanical Engineering Department, ENS Paris-Saclay
4 Avenue des Sciences, 91190 Gif-sur-Yvette, France

e-mail: benjamin.gat, octave.jeanne, emmanuel.baranger@ens-paris-saclay.fr

KEYWORDS: Supervised Learning; Thermodynamics; GENERIC formalism; Gated Recurrent Unit.

ABSTRACT

General Context

This study was motivated by thermodynamics behaviors of materials which are being modeled on a case-by-case basis. A part of the mechanical research community is studying neural network to find general approximators to model complex mechanical behaviors. However, classical neural networks are not constrained to follow laws of physics. Most of the current solutions to this problem is to penalize the loss function used to train the model when the predictions are not thermodynamically consistent [1] or to use classification to select the most relevant existent models [2]. Our work aims at enforcing the thermodynamical consistency directly in the structure of a neural network.

Methods

The first part of the project was to choose a dynamic model that respects the fundamental laws of thermodynamics. The General Equation for the Nonequilibrium Reversible-Irreversible Coupling (GENERIC) formalism [3] was adopted due to its compacity. This model is based on a first order Ordinary Differential Equation (ODE) that rules the time evolution of the state variables :

$$\frac{d\underline{x}}{dt} = L\frac{\partial E}{\partial \underline{x}} + M\frac{\partial S}{\partial \underline{x}} \qquad (1)$$

with $\underline{x}$ the state variables , L the Poisson matrix, M the Ginzburg-Landau matrix, E the energy potential and S the dissipation potential.

In addition, the model provides consistency with the first law of thermodynamics by imposing the following properties:

$$L = -L^T \; ; \; \frac{\partial E}{\partial \underline{x}} \in ker(M) \qquad (2)$$

Moreover, the model enforces the second law of thermodynamics using the following properties:

$$M = M^T \; ; \; \frac{\partial S}{\partial \underline{x}} \in ker(L) \; ; \; M \; is \; positive - definite \qquad (3)$$

The second part of the project was to select a neural network architecture compatible with the form of the equation (1). Niu's work [4] suggests that Gated Recurrent Units (GRUs) are comparable to the Runge-Kutta integration scheme. This scheme is adapted to solve matricial first order ODEs which is the type of equation (1). Thus, the GRU structure was chosen for this model.

The final part of the project was to implement the constraints (2) and (3) in a neural network architecture. We provided a neural network structure composed of two branches. The first one is meant to predict the Poisson matrix and the gradient of the system's dissipation potential respectively to the state variables. The second one is meant to predict the Ginsburg-Landau matrix and the gradient of the system's energy potential respectively to the state variables. Only the second branch was implemented in the project. The symmetry and degeneracy properties of the GENERIC operators were enforced directly in the branch structure through custom activation functions connecting three sub-FCNNs.

Results

Results on the study of GRU structures show that the formatting of inputs changes the way the information is processed by the network. Additionally, a large dependence of the outputs on the hyperparameters was found. Finally, the equivalence between the Runge-Kutta scheme and the GRU architecture was able to provide weights and biases that allowed the GRU to accurately approximate a function ruled by a first order ODE.

The thermodynamic admissibility of the data provided by the GENERIC informed neural network is being tested regardless of the system to model. In parallel, the model is also being trained and tested on the behavior of a system constituted of a mass attached to a spring and a damper.

Further Works

After obtaining and interpreting more results of the evaluation of the GENERIC informed neural network, the first next step will be to find a way to avoid local minima in its training. Once this is done, the following step will be to implement the branch providing the Poisson matrix and the gradient of the dissipation potential. The final step will be to implement the GENERIC-informed structure in a larger GRU structure in order to dynamically predict the behavior of a complex mechanical system.

References

[1] Q. Hernández et al. Structure-preserving neural networks. *Journal of Computational Physics.* **Vol**:426, 1 February 2021.
[2] K. Linka, E. Kuhl. "A new family of constitutive artificial neural networks towards automated model discovery". *Computer methods in applied mechanics and engineering.* **Vol**:403, January 2023
[3] M.Grmela, H.Öttinger. Dynamic and thermodynamics of complex fluids. I Development of a general formalism. Physical Review volume 56 number 6. 1997.
[4] M.Y. Niu, I.L. Chuang, L. Horesh. Recurrent Neural Networks in the Eye of Differential Equations. *arXiv:1904.12933v1*, 2019.

Autonomous cars : Automated Driving and safety

J. BESNARD - A. HUVELLE - G. FARAUT

TER M1 2023-2024

FINAL DEFENCE OF RESEARCH PROJECTS

April 2, 2024, Gif-sur-Yvette, France

école normale supérieure paris-saclay

TER M1 2023-2024
FINAL DEFENCE OF RESEARCH PROJECTS
April 2, 2024, Gif-sur-Yvette, France

Autonomous cars : Automated Driving and safety

Jay Besnard*, Armand Huvelle*, Grégory Faraut*◊

* Department of Mechanical Engineering
University Paris-Saclay – Ecole Normale Supérieure Paris-Saclay
4 avenue des sciences, 91190, Gif-sur-Yvette
e-mail: Jay.besnard@ens-paris-saclay.fr.fr, Armand.huvelle@ens-paris-saclay.fr
◊e-mail: Gréegory.Faraut@ens-paris-saclay.fr

KEYWORDS: Discret Event System; Autonomous Vehicle; Security.

ABSTRACT

Introduction

In the paradigm of autonomous vehicles, the exploration of their control and resilience in the face of potential cyber-attacks has become increasingly crucial. Consequently, our study aims to address this topic from a DES perspective. Initially, we were equipped with a remote-controlled car fitted with a single lidar sensor, which allowed us to conduct our initial study, particularly in terms of control based on AI methods. Subsequently, we evolved this setup into a vehicle equipped with omnidirectional wheels, better suited to our research. The theses of Salah Eddine Ghamri [1] and Benoit Thuilot [2] enabled us to establish a state-of-the-art understanding of the subject.

1 Integration of Reinforcement Learning-Based Control Methods

The initial vehicle in our study, equipped with a Lidar, operates through a Raspberry Pi 4 nano-computer, which we had to familiarize with. Initially, we ran it with basic code that allowed us to conduct our initial experiments. We also familiarized with the Webots simulation software using the same basic code.

Subsequently, we delved into an AI-based reinforcement learning approach that we successfully implemented on Webots. Drawing upon established research in reinforcement learning from the ENS EEA department, the strategy we then adopted involves a reward function, crucial for the autonomous vehicle's learning, assigning rewards based on the vehicle's current state. It distinguishes between collision and non-collision states, penalizing collisions with a point penalty and providing rewards based on speed and distance to obstacles detected by the lidar. The neural network architecture used in our study comprises an input layer of 360 neurons corresponding to the lidar values and two output neurons representing speed and direction commands.

2 Behavior Model (DES)

Initially, we made some assumptions to establish the behavior automaton of the holonomic car. Firstly, we considered that each wheel could move forward, backward, or stay stopped. We did not address the problem from a hybrid systems perspective, so speed changes will be discrete rather than continuous. Also, we chose a single constant speed applicable for both forward and backward movement. In this case, the car's movements are limited to ten. Finally, we assumed that the lidar

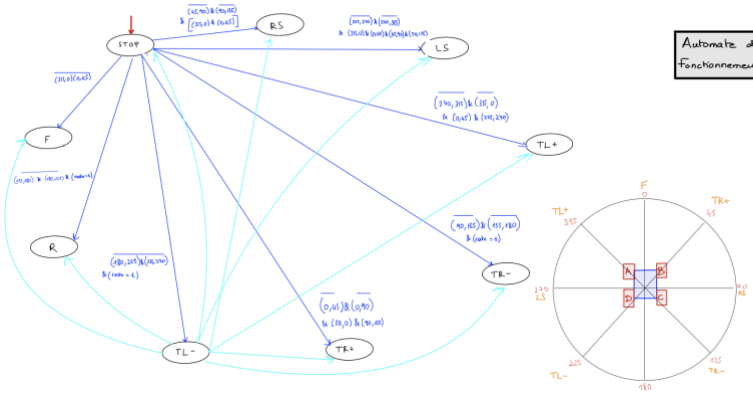

Figure 1: Control plant

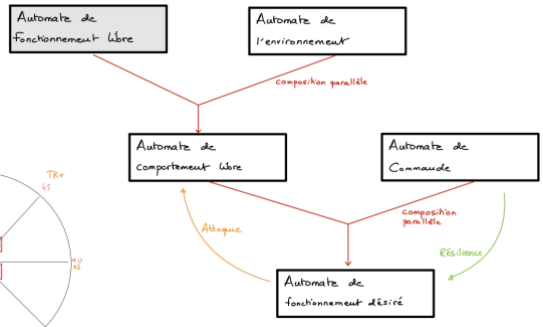

Figure 2: Parallelization diagram

Additionally, we only considered the following eight sectors: (0-45°); (45-90°); (90-135°); (135-180°); (180-225°); (225-270°); (270-315°); (315-0°). These assumptions simplify the problem to make it more understandable and manageable. However, it is possible to disregard each of these assumptions by considering all lidar values and continuous speed changes, which would significantly increase the number of states for each automaton.

To model the behavior of this vehicle, we chose to create three plants. The first model free operation by considering all possible combinations of states of the four wheels, totaling (3^4) 81 states. The second models the environment by representing all possible combinations of the eight lidar sectors, totaling (2^8) 256 states. The last one represents the control of the car (Fig 1) by positioning itself as a specification of the free operation plant. We then seek to achieve the parallelization summarized in Figure 2 to obtain the vehicle's control.

3 Definition of Cyberattack and Resilience considering our Model

Building upon two theses [3][4], we have decided to start by identifying the defended and weakly defended states of the desired operation. The attack we defined involves going through the paths of the automaton that are closest to the weakly defended states with the aim of increasing the chance of a breakdown or malfunction that could lead to damage the vehicle. Conversely, the resilience of the control involves going through the paths furthest from the defended states to limit any unexpected behavior. Additionally, resilience involves adapting the control in an event of breakdown or damage, such as a blocked wheel. In this case, we aim to adjust the control to maintain the right behavior that is less optimized but still functional.

4 Perspectives

In the future, we aim to implement the practical application of the attack and resilience vision of the control that we have both defined. This involves, for example, adapting the control law to a three-wheeled vehicle instead of four. Similarly, we intend to simulate this concept using the Webots software by programming a four-wheeled holonomic car, enabling us to test our controller.

REFERENCES

[1] Salah Eddine Ghamri *Commande Neuronale d'un Robot Mobile Non-Holonome avec glissement des roues,* 2015

[2] Benoit Thuilot *Contribution à la modélisation et à la commande de robots mobiles à roues,* 2013

[3] Samuel Oliveira, André B. Leal, Marcelo Teixeira, Yuri K. Lopes *A classification of cybersecurity strategies in the context of Discrete Event Systems*, 2023

[4] Rong Su *On Decidability of Existence of Nonblocking Supervisors*, 2022

Development and processing of tests on a biaxial compression Hopkinson bar system.

G. JAUZE - X. KERSTEL - B. DURAND

TER M1 2023-2024

FINAL DEFENCE OF RESEARCH PROJECTS

April 2, 2024, Gif-sur-Yvette, France

école normale supérieure paris—saclay

Development and processing of tests on a biaxial compression Hopkinson bar system.

Jauze Grégoire, Kerstel Xander, Durand Bastien

Génie Mécanique
ENS Paris-Saclay
e-mail: gregoire.jauze@ens-paris-saclay

Génie Mécanique
ENS Paris-Saclay
e-mail: xander.kerstel@ens-paris-saclay

LMPS
ENS-paris-saclay
e-mail: bastien.durand@ens-paris-saclay

KEYWORDS: dynamic; biaxial; compression.

ABSTRACT

Accounting for impacts during the design of dynamic systems is very important. Dynamic compression and tensile test benches, such as Split Hopkinson Pressure Bars can address such questions. However, these tests do not account for biaxial loads, which are frequently encountered in practical situations. Therefore there is a need to conduct biaxial dynamic compression tests. Here we describe our efforts to master a system capable of biaxial loading of a specimen.

Similar tests have already been carried out at the LMPS with a standard Split Hopkinson Pressure Bar and a device that would convert a part of an axial force to a tangential force, but the force on the second axis depended on the friction between parts, which made it hard to interpret the results accurately[1].

A purely biaxial machine was developed at the Northwestern Polytechnical University (China), using magnetic cannons to propel steel bars at a very precise instant and a precise speed [2]. However the machine is entirely made of titanium to avoid unwanted magnetic effects. The use of titanium and magnetic cannon make it rather expensive.

The system developed at the LMPS uses a single projectile, and splits the shock wave along four bars to create four incident waves arriving simultaneously on the sample. Our objective in this project is to make sure that this machine is functioning well: the load should be equal on all axes, and the measurements should correspond

to the theory. For this, we test samples made of aluminium (Fig.1), which has a known and predictable biaxial dynamic behaviour. Displacement is measured by Digital Image Correlation. In addition, strain gauges combined with wave propagation theory allow us to calculate the speed and the stress at the end of the bars. It is thus possible to indirectly measure the force and displacement applied to each face of the sample. We should find that the strain-stress response we get with the machine coincides with the numerical simulation obtained via Abaqus.

To verify that the load is equal along both axes, we compare the results obtained with the strain gauges. We found that they were very similar (Fig.2). To check that the material behaviour was correctly Identified, we test the sample material to get its uniaxial behaviour. We can then input it in Abaqus and verify that the simulation corresponds to the measurements.

RÉFÉRENCES

[1] Bastien Durand, Pierre Quillery, Ahmed Zouari, Han Zhao. Exploratory Tests on a Biaxial Compression Hopkinson Bar Set-up. *Experimental Mechanics* **61**: 419–429, 2020.

[2] Kanghua Jin, Lin Qi, Huaipu Kang, Yazhou Guo, Yulong Li. A novel technique to measure the biaxial properties of materials at high strain rates by electromagnetic Hopkinson bar system. *International Journal of Impact Engineering* **167**: 104286, 2022.

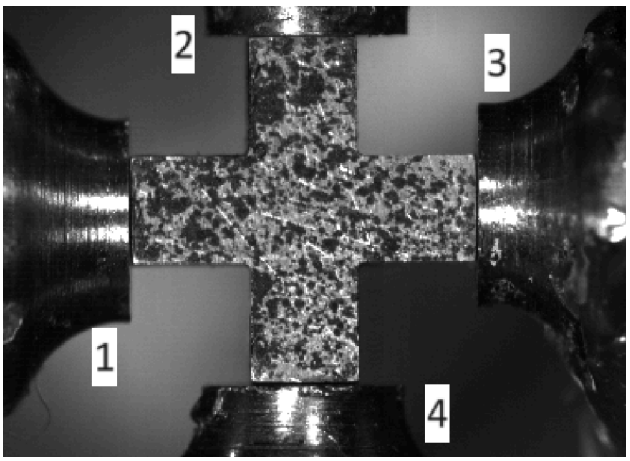

Fig.1 : Aluminum sample hold between the bars. Each branch is 2.7 mm wide.

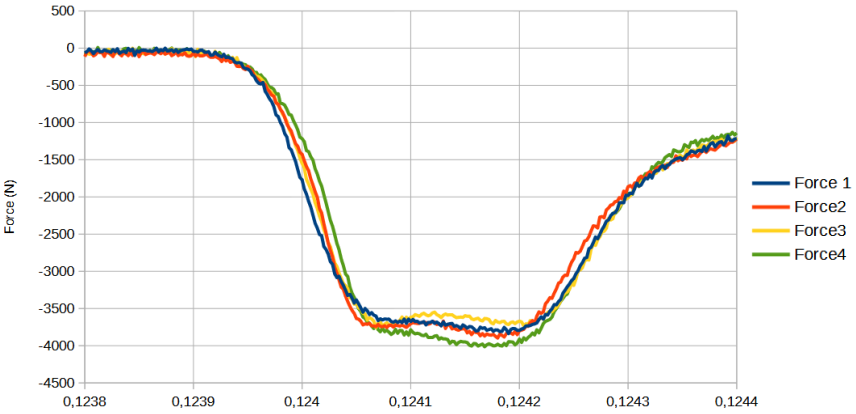

Fig.2 : Forces obtained with the strain gauges as a function of time

Construction of a homogenized mechanical model for a disordered optical fiber coil

T. CLEMENT - P. JEGOU - F. LOUF - P. BUSNEL

TER M1 2023-2024

FINAL DEFENCE OF RESEARCH PROJECTS

April 2, 2024, Gif-sur-Yvette, France

école normale supérieure paris—saclay

Construction of a homogenized mechanical model for a disordered optical fiber coil

T. Clément [a], P. Jegou [a], F. Louf [b], P. Busnel[b,c]

a. DER de Génie Mécanique, ENS Paris-Saclay, 91190, Gif-sur-Yvette, France.

b. Université Paris-Saclay, CentraleSupélec, ENS Paris-Saclay, CNRS, LMPS - Laboratoire de Mécanique Paris-Saclay, 91190, Gif-sur-Yvette, France.

c. Exail, 78100 Saint-Germain-en-Laye, France.

email: {tom.clement, pierre.jegou, francois.louf, pierre.busnel}@ens-paris-saclay.fr

KEYWORDS: FOG; Homogenization; RVE.

ABSTRACT

General Information

Inertial navigation systems are extremly useful to navigate, especially under water. Those using Fibre Optic Gyroscopes (**FOG**) are the most effective yet. However, their manufacture requires coils and knowledge of their caracteristics is important as an error in the measure and interpretation of the optical signal may result in a submarine emerging miles from the location wanted. Furtheremore, to reach high precision, coils are made ordonned which severly reduce the thermal bias. However, the manufacture of ordonned coils can only be achieved trough sheer manpower and cannot be replaced by machines yet. Hence the use and the thermal bias of non-ordonned coils assembled automatically is studied.
It has been shown [1] that ordonned coils properties tend to varry alongside the temperature, this generates a thermal bias and some strain influencing the optic propagation. An axisymetric hypothesis was used but each spire was considered. **Homogenization** was conducted [2] in order to reduce the workload of the computer and compared to the "exact" solution to mesure the trust interval. The idea is now to execute a **homogenization** upon a non-ordonned coil to see the difference with an ordonned one and then to measure the mechanical characteristics and the new thermal bias. This will allow to caracterize the precision a **FOG** can get with a disordered coil in comparaison to an ordonned one.

Method

Firstly, a tomography of a disordered coil was made. Then, from images taken out of it, corresponding to different sections, the center of each spire were extracted in order to make a numerical model of the coil and run calculations with it. Everything was calculated under the software Cast3M in a section with axisymetric and homogeneous periodicity hypotheses. Due to the resolution of the tomography and to residual strain, fibers may intersect. Pre-processing is needed in order to create the circles. Once this is done, a small piece of the section (**RVE**) was meshed automatically using the fibers' center (see **Figure 1(b)**). Then, an **homogenization** method was conducted why the previously estated hypotheses. At last, the **RVE** size and location can be changed to try to find the most representative one. The implementation of the **RVE** was used to caracterize the dispersion of every caracteristics and because of the large number of fiber per section, an automatization of the different simulations was mandatory to scan the whole section. It was firstly done only with the compacity, being simpler and faster to calculate because the only data needed is the surface of the mesh of the glue and the total one(see **Figure 1(a)**), explicitly the formula is $C = 1 - \frac{S_{glue}}{S_{RVE}}$. It was calculated this way as the glue surface is given by a single mesh, and the **RVE** is generally a rectangle.

Results

The data extracted allowed to get an average value and its dispersion for different caracteristics. The following table discribes it all (see **Table 1**). It is to be considered that the compacity is effective, i.e. it

is divided by the maximal compacity obtainable (hexagonal close-packed : 0.74). It is interesting to see that the influence of the z-axis is less important than the r-axis on the coil. The use of a smaller **RVE** seems mandatory as the dispersion is less important. It is not intuitive but it seems a larger RVE does not implies better precision.

Further work

In order to have a greater idea of the comportement of disordered coils, a study of a larger number of these can be considered. Considering that making tons of tomography of disordered coils is impossible for reasons of time, generating them by computer is a path that can be explored in the future. The challenge would be to create controlled disorder in a coil to produce a large number of sample and have a statistic distribution of the comportement of those which then could be compared to a few tomographies of real disordonned coils.

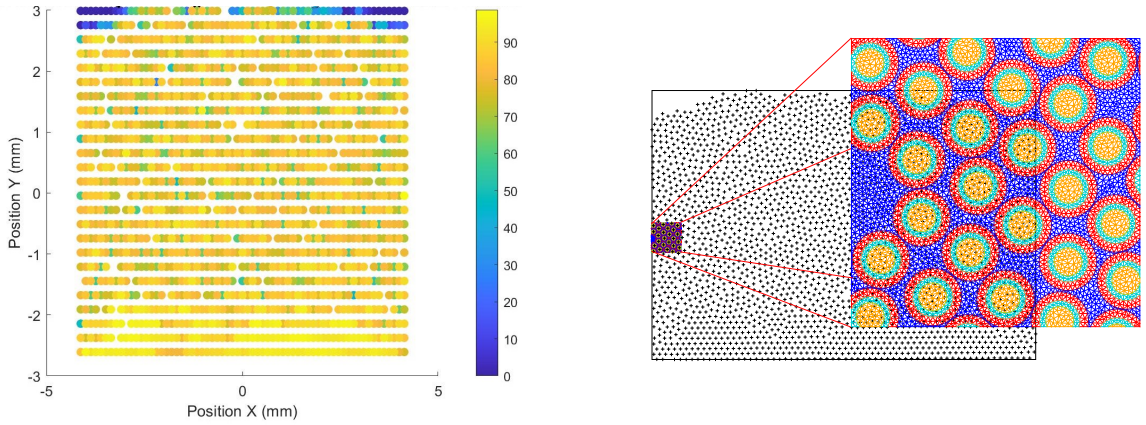

(a) (b)

Figure 1: (a) : Spacial repartition of compacity with a rectangular **RVE** of 1x$\sqrt{3}$ diametre of fibre. (b) : Meshing of a **RVE** of 5x5 diametre of fibre in a section.

Property	Value	Coefficient of variation (%)	dispersion Z (%)	dispersion R (%)
$E_{xx}(GPa)$	25.4 / 19.2	33.2 / 22.9	7.06 / 37.9	11.9 / 32.9
$E_{yy}(GPa)$	25.8 / 18.1	39.9 / 22.9	3.44 / 11.5	11.9 / 44.6
$E_{xy}(GPa)$	8.86 / 6.70	50.4 / 29.3	4.59 / 8.16	16.5 / 50.4
ν_{xy}	0.248 / 0.300	14.6 / 14.3	1.84 / 5.99	5.76 / 13.4
ν_{yx}	0.255 / 0.282	25.6 / 20.3	5.46 / 5.30	11.0 / 24.5
Compacity	82.2 / 70.2	27.9 / 9.3	1.96 / 18.7	5.20 / 31.5

Table 1: Property values and dispersion of two different RVE size, 1×$\sqrt{3}$ and (/) 5×5.

REFERENCES

[1] J.Pillon, Matthieu Collignon, M. Rattier, F.Louf, Emmanuelle Peter, Pierre-Alain Boucard and Hervé C. Lefèvre. Three-Dimensional Topological Reconstruction of the Sensing Coil of a Fiber-Optic Gyroscope Using X-Ray Computed Tomography. JOURNAL OF LIGHTWAVE TECHNOLOGY, **VOL**.39, **NO**.14, July 2021.

[2] P.Busnel, J.Pillon, F.Louf, M. Rattier, Pierre-Alain Boucard. Développement d'un Modèle Thermomécanique Homogénéisé pour la Conception Optimisée de Gyromètres à Fibre Optique. 2022.

Structure of human collagen fiber organization in connective tissues

N. MOREL - M. LE STRAT - E.BUDYN

TER M1 2023-2024

FINAL DEFENCE OF RESEARCH PROJECTS

April 2, 2024, Gif-sur-Yvette, France

école normale supérieure paris–saclay

TER M1 2023-2024
FINAL DEFENCE OF RESEARCH PROJECTS
April 2, 2024, Gif-sur-Yvette, France

Structure of human collagen fiber organization in connective tissues

N. Morel*, M. Le Strat†, E.Budyn◇

Department of Mechanical Engineering
Ecole Normale Supérieure Paris-Saclay, University Paris-Saclay
*e-mail: nathan.morel@ens-paris-saclay.fr
† e-mail: maxime.le_strat@ens-paris-saclay.fr
◇ e-mail: elisa.budyn@ens-paris-saclay.fr

KEYWORDS: Cortical bone; Osteocyte; Collagen fiber; Composite; Mechanical constitutive law.

ABSTRACT

Introduction

Bone is a complex material and grows differently depending on the stress it undergoes. Knowledge on internal stress applied on the osteocytes is essential for a better understanding of degeneration associated with it [3]. We will study the properties of the REV (Representative Elementary Volume) of bones and stress in different phases.

Materials and Methods

The REV studied is based on a segmentation of fluorescent confocal microscopy observations [3]. A previous model including materials with linear properties has been made on Abaqus. The aim of this study is to adapt this model to include non-linear properties to have a better representation of real-life bones.

Fiber orientation of collagen in the osteon influences the behavior of the REV drastically. Indeed, the bone matrix adapts to its mechanical environment. In particular, longitudinally-oriented collagen is more present in tension areas whereas oblique-angled fibers are more present in compression areas [2]. Therefore, we studied a model with collagen fibers oriented at 45° and 135° while the other group studied collagen fibers oriented at 60° and 120°. We compare our results with an imposed constraint at the limit strain of homeostasis : 1.5 micro-strain under compression and 1 micro-strain under tension [1].

The organisation of collagen fibers has a paramount significance on bone mechanical properties [4]. That's why this study focuses on a geometrical complex REV to make it as close as possible to real-life bones.

Results and discussions

We obtain results for materials with a linear behaviour. As shown on figure 1, calculated stresses are projected on a unit sphere to visualize main directions of stresses in different phases.

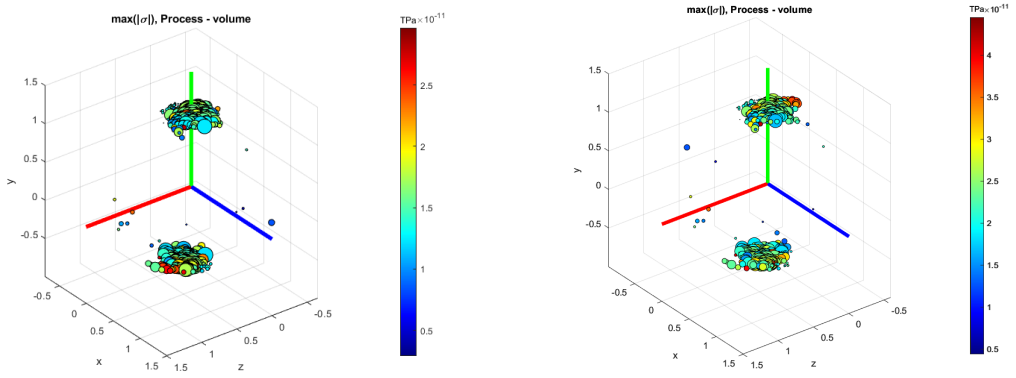

(a) Tension (b) Compression

Figure 1: Representation of the maximum of the absolut value of stress and its direction

We can observe that either in tension or in compression, the hydroaxyapatite (HAP) takes the most of the stress. It seems logical because HAP is the more rigid phase. We also notice that the main direction is colinear to the y axis, that is consistent with our boundary conditions which are also, in tension and in compression, colinear to the y axis.

Under 1.5 compressive micro-strain of the REV, the cell process is under a minimal principal stress of -5 to -45 Pa compression and a maximum principal stress in mixed mode of 2 Pa tension and 10 Pa compression.

Under 1 tensile micro-strain of the REV, the cell process is under a minimal principal stress of -25 Pa to 10 Pa compression and a maximum principal stress in mixed mode of 30 Pa tension and 7 Pa compression.

The strains are higher in compression than in tension. Regarding the limit strain under compression and tension, the REV will be as resistant in compression as in tension.

REFERENCES

lalilalalilaR. Al Nazer, J. Lanovaz, C. Kawalilak, J.D. Johnston, S. Kontulainen. Direct in vivo strain measurements in human bone—A systematic literature review. *Journal of Biomechanics* **Vol**:45 27-40, 2011. Kilian E. Stockhausen, et al. Collagen Fiber Orientation Is Coupled with Specific Nano-Compositional Patterns in Dark and Bright Osteons Modulating Their Biomechanical Properties. *ACS Nano* **Vol**: 15, 2021 E. Budyn. A Bone-on-Chip as a 3D in Vitro Platform to assess the Effect of Stem Cell Age on Tissue Quality and Test Medicines. *Tissue Engineering: Parts A, B, and C.* **Vol**:29 13-14, 2023. Georgiadis M, M*ü*ller R,Schneider P. 2016 Techniques to assess bone ultrastructure organization: orientation and arrangement of mineralized collagen fibrils.*J. R. Soc. Interface* **Vol**:13, May 2016

Fracture mechanic of architectured materials

C. ROGIER – C. LELONG – F. DAGHIA

TER M1 2023-2024

FINAL DEFENCE OF RESEARCH PROJECTS

April 2, 2024, Gif-sur-Yvette, France

école normale supérieure paris–saclay

TER M1 2023-2024
FINAL DEFENCE OF RESEARCH PROJECTS
April 2, 2024, Gif-sur-Yvette, France

Fracture mechanic of architectured materials

Clément Rogier*, Chloé Lelong†, Federica Daghia◇

* † ◇ Mechanical engineering department
ENS Paris-Saclay
4 avenue des sciences, 91190 Gif-sur-Yvette
*e-mail : clement.rogier@ens-paris-saclay.fr and †e-mail : chloe.lelong@ens-paris-saclay.fr
and ◇e-mail : federica.daghia@ens-paris-saclay.fr

KEYWORDS: fracture mechanics, metamaterials, octet-truss.

ABSTRACT

Introduction

Architectured materials are investigated for the great mechanical characteristics they can achieve by combining the properties of their parent materials with their microstructure. Here, we focus on the study of lattice-based architectured materials, which consists of bars connected by nodes. In particular, we study the octet-truss lattice (see Fig.1). While elastic properties of such architectured materials have been widely investigated in the literature [Deshpande 2001], only few papers studied their fracture behavior and their behavior under localized load. Here, we aim to develop the framework required to simulate the fracture of lattice-based architectured materials, in order to characterize the crack propagation in such architectured materials through an energetic approach.

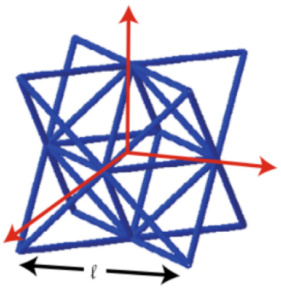

Fig 1. - Octet-truss

Foundation and validation of the model

In order to perform cracking and indentation calculations on our architectured material, the first step was to create the mesh of our structure. To achieve this, we used the coordinate transformation principle of the finite element method, which enabled us to project and repeat the octet-truss cell on the mesh of a solid in `.inp` format from Abaqus. This method has the advantage of being able to generate meshes, from regular to more complex shapes, of cracked architectured materials automatically.

Then we compared our simulations with the literature to verify its stiffness [Deshpande 2001] and normalized toughness [Deshpande 2022]. In both cases, we simulated tensile tests on specimens made of a parent material, assumed to be linearly elastic, by imposing nodal forces. To estimate stiffness, we measured displacements in a cubic specimen, whereas to determine the toughness of our material, we measured the maximum of the Von-Mises stress field in a cracked sample. The estimated stiffness and toughness values are in accordance with the literature [Deshpande 2001, 2022].

Results on the study of a sample under localized load, and of the stress distribution for a cracked sample

During the study of this architected material, we were expecting scale effects on our results. Therefore, we decided to perform indentation simulations where we plotted the stiffness evolution with the number of cells under imposed displacement in an Octet-truss structure. We carried out two sets of simulations : the first one in 2 dimensions (see Fig. 2) and the second one in 3 dimensions. The stiffness convergence, where the macroscopic stiffness is constant, allowed us to observe the influence of the microstructure's size and its organization.

We have performed an explicit elastic dynamics calculation on Abaqus to study the progressive fracture of a sample made from an architectured material. To do this, we added a brittle-cracking behavior to the material, in which we specified the strain-stress profile at failure. We worked with imposed displacement. To accelerate the calculation, we used mass scaling, which consists in changing the mass over time. However, the dynamic behavior has an effect on the energy redistributed to bars and the mass scaling distorts results as bar masses are no longer correct.

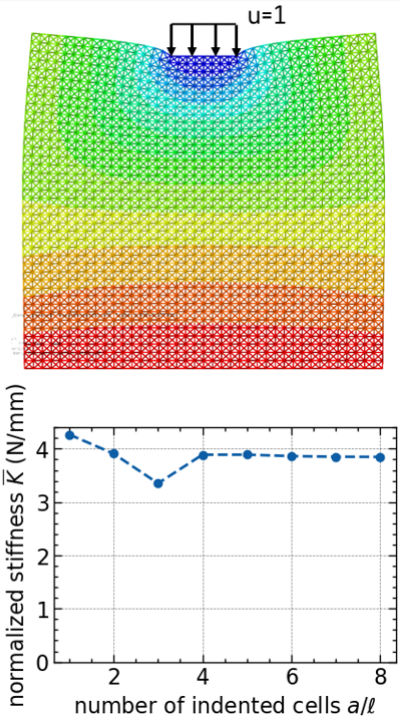

Fig 2. - Model and results of the 2D indentation simulation

Conclusion

We have partially developed the tools needed to study localized loading and crack propagation in lattice-based materials. The results obtained so far are in line with the literature. To continue the study, we would like to use a house code, which allows us to progressively remove each bar one by one every time they crack instead of a dynamic calculation, so as to be able to study material characteristics in greater detail from an energetic point of view.

REFERENCES

[1] V.S. Deshpande, N.A. Fleck, M.F. Ashby. Effective properties of the octet-truss lattice material. *Journal of the Mechanics and Physics of Solids* **49**:1747-1769, 2001.

[2] V.S. Deshpande, et al. The toughness of mechanical metamaterials. *Nature materials* **21**:297-304, 2022.

Characterization of Electrical Consumption in Laser Wire Additive Manufacturing for Sustainable Development

A. BLALATE - T. LEGLISE - N. MULLER – C. TOURNIER

TER M1 2023-2024

FINAL DEFENCE OF RESEARCH PROJECTS

April 2, 2024, Gif-sur-Yvette, France

école normale supérieure paris–saclay

TER M1 2023-2024
FINAL DEFENCE OF RESEARCH PROJECTS
April 2, 2024, Gif-sur-Yvette, France

Characterization of Electrical Consumption in Laser Wire Additive Manufacturing for Sustainable Development

A. BLALATE*, T. LEGLISE*, N. MULLER◇ , C. TOURNIER ◇

Mechanical Engineering Department, LURPA
École normale supérieure Paris-Saclay
4 avenue des Sciences, 91190 Gif-Sur-Yvette, France
e-mail: {firstname.lastname}@ens-paris-saclay.fr

KEYWORDS: Additive Manufacturing; Specific Energy Consumption; Sustainability.

ABSTRACT

The advent of additive manufacturing gives the ability to print complex geometries and offer efficient solutions for maintenance and repair [1]. The wire laser additive manufacturing (WLAM) process uses a laser to melt a metal wire, adding layers to create the geometry. Hence, environmental impact is leading the industry to develop sustainability policies such as the European Union 2050 Green Deal. This study seeks to establish the specific energy consumption (SEC) of the WLAM process and to determine optimised strategies.

$$SEC(P_{laser}, V_{head}, V_{wire}, Z_{height}, ON/OFF_{servo-control}) = \frac{E_{tot}[\text{kWh}]}{m_{product}[\text{kg}]} \quad (1)$$

Energy consumption models exist for similar technologies, but to date, they are currently scarce compared to models for machining [3]. Previous studies have shown the importance of considering more appropriately the additive process which is not easily comparable with subtractive processes [2]. Few previous papers have investigated on the characterization of the different sub-systems and process stages [4, 5]. This work focuses on modeling energy consumption by collecting data from the different life cycles and equipment, considering the phases of rest, rapid movement, elementary trajectory and pause, each temporally weighted.

Each consumption of subsystems were measured (Figure 1) using a power sensor (FLUKE 434) and modelled with constant or linear functions. A test was performed without servo control, using main and auxiliary equipment for a single bead wall ($100 \times 100 \times 2.95$). A SEC of 17.52 $kWh.kg^{-1}$ was calculated thanks to our model (Figure 1). The results suggest that the laser power consumption is an important factor in the linear variation in electricity consumption. Our findings indicate that by activating the laser servo-control the energy consumption can be reduced to 16.6 $kWh.kg^{-1}$. Moreover, the use of higher laser power and faster printing speeds enable to achieve 15.19 $kWh.kg^{-1}$ due to the limited

running time of auxiliary equipment. These calculated values are ranked in the lower range according to previous studies that have evaluated SEC for additive processes [2].

Overall, our findings support the assumption that auxiliary equipment consumption is a significant issue. Improvements might be possible by increasing speed and laser power in order to keep the linear energy constant. The study guides recommendations for the overall energy strategy of the additive manufacturing cell towards optimising the time spent outside the deposition phase. Future studies should assess optimised strategies using a preheated wire and servo-control laser power monitoring.

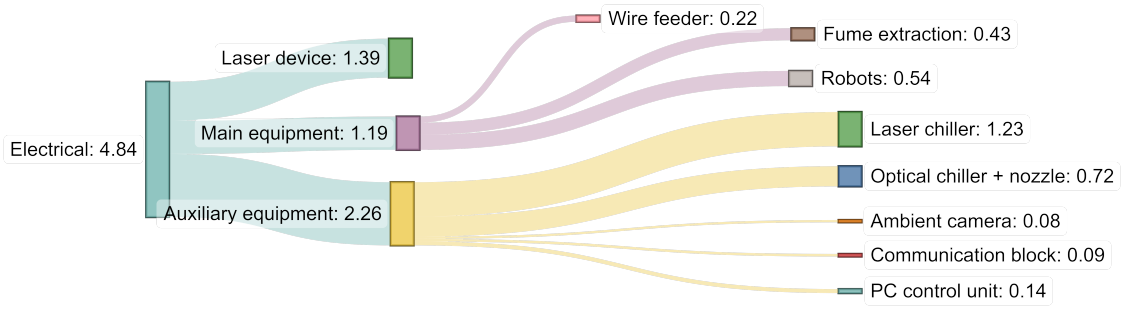

Figure 1: WLAM energy flow (kWh) (standard strategy: laser at 2200 W)

REFERENCES

[1] Z.Y. Liu, C. Li, X.Y. Fang, Y.B. Guo, Energy Consumption in Additive Manufacturing of Metal Parts, Procedia Manufacturing, 26:834-845, 2018.

[2] HS. Yoon, JY. Lee, HS. Kim et al., A comparison of energy consumption in bulk forming, subtractive, and additive processes: Review and case study, Int. J. of Precis. Eng. and Manuf.-Green Tech. 1:261–279, 2014.

[3] S. Kara, W. Li, Unit process energy consumption models for material removal processes, CIRP Annals, 60(1):37-40, 2011.

[4] N. Goffin, L. C. R. Jones, J. Tyrer, et al., Characterisation of laser system power draws in materials processing, Journal of Manuf. and Materials Processing, 4(2):48-65, 2020.

[5] M. Baumers, C. Tuck, DL. Bourell et al., Hague, Sustainability of additive manufacturing: measuring the energy consumption of the laser sintering process, Proceedings of the Institution of Mechanical Engineers, J. of Eng. Manuf. 225(12):2228-2239, 2011.

Acknowledgments to Phillipe Cornet for his help to power measurements

Non-linear vibration analysis of an axial compressor blisk of an aircraft engine.

T. MAUBERT – M.MILANESI-GIRAUDO – J. ARMAND – Q. MERCIER – F. FEYEL

TER M1 2023-2024

FINAL DEFENCE OF RESEARCH PROJECTS

April 2, 2024, Gif-sur-Yvette, France

école normale supérieure paris–saclay

TER M1 2023-2024
FINAL DEFENCE OF RESEARCH PROJECTS
April 2, 2024, Gif-sur-Yvette, France

Non-linear vibration analysis of an axial compressor blisk of an aircraft engine.

T. Maubert*, M. Milanesi-Giraudo†, J. Armand◇, Q. Mercier◇, F. Feyel◇

*†Mechanical Enginnering Department
École Normale Supérieur Paris-Saclay
4 Avenue des Sciences, 91190 Gif-sur-Yvette
*e-mail: thibault.maubert@ens-paris-saclay.fr
† e-mail: maceo.milanesi-giraudo@ens-paris-saclay.fr

◇ Safran Tech
Rue des jeunes Bois, 78112 Magny-les-Hameaux France
e-mail: jason.armand@safrangroup.com, quentin.mercier@safrangroup.com &
frederic.feyel@safrangroup.com

KEYWORDS: Vibration; Nonlinear Analysis; Harmonic Balance Method.

ABSTRACT

Context and Introduction

The bladed disks of a turbomachine are subject to numerous vibrations caused by the behavior of air within it. In order to extend their lifespan, the vibrational response of the disks must be understood and attenuated. To control this, the chosen technological solution in single-block high-pressure compressors is a pre-loaded ring damper mounted at the central bore (see Figure 1). However, its sizing is complex and remains highly simplified in the literature. The strongest assumption consistently made in the literature is the cyclic symmetry of the problem. This assumption implies neglecting the actual shape of the ring, which, for assembly reasons, is cut. This therefore implies a non-homogeneous pressure between the disk and the ring, which, to our knowledge, has not been taken into consideration [3].

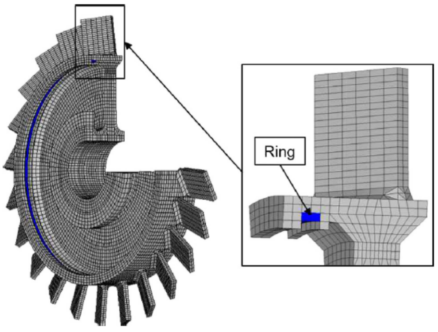

Figure 1: The ring and its placement within the disk.
Baek and Epureanu, Reduced-Order Modeling of Bladed Disks With Friction Ring Dampers, 2017

Method

Based on the Laxalde model proposed in [1], a phenomenological analysis of the impact of the uniform contact pressure assumption is suggested. A lumped model based on the latter

model, with a ring damper cut off, is proposed to find an initial solution of forced response in HBM (Harmonic Balance Method proposed in [2]), based on an assumption of a uniform pressure field between the ring damper and the disk (see Figure 2). However, this assumption is not statically admissible in the case of cutting. Initially, the field is approximated by a statically admissible field where the efforts of the missing ring sector are fully taken up by the neighboring sectors. This new assumption in the first lmuped model then allows for finding a new, more realistic solution of forced response in HBM.

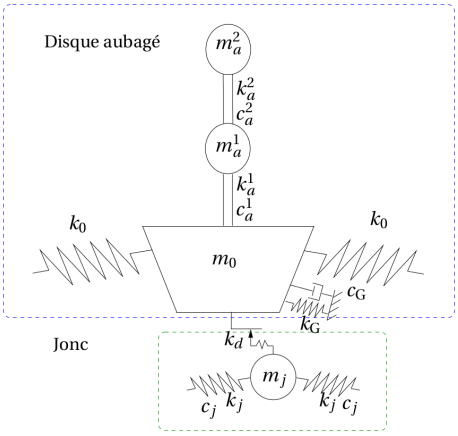

Figure 2: Lumped model in [1]

At the same time, a finite element model of the assembly is constructed based on the actual geometry of the system using Abaqus to find a more representative contact pressure field through static nonlinear analysis. Thus, this new pressure field implemented in the lumped model presented in the previous section allows for finding a third solution of forced response in HBM, enabling the measurement of the impact of load distribution between the ring and the disk. As a comparison, a calculation using the finite element model with time integration is performed to serve as a reference solution.

Key results and interpretations

The importance of the type of pressure field in the lumped model is highlighted in the various simulations conducted. The mistunning effects introduced by heterogeneous pressure fields are minimal with the first assumption. Once the flexibility of the ring damper is taken into account, the distribution of contact pressures concentrates on the sectors adjacent to the cut and the diametrically opposed sector while unloading the other sectors. This distribution accentuates the mistunning effects, displaying it as equally influential as the cut itself, and when these effects are compounded with those of the cut, the mismatch intensifies. This suggests that it is important when designing ring dampers to consider these pressure distributions.

REFERENCES

[1] D. Laxalde, Étude d'amortisseurs non-linéaires appliqués aux roues aubagées et aux systèmes multi-étages, 2007.

[2] M. Krack, J. Gross. *Harmonic Balance for Nonlinear Vibration Problems*. Spinger, 2019.

[3] S. Gao, Y. Wang. An Evaluation Method for Dry Friction Damping of Ring Damper in gas Turbine Engines under Axial Vibration. *Aerospace* **8**:302, 2021.

TER M1 2023-2024
FINAL DEFENCE OF RESEARCH PROJECTS
April 2, 2024, Gif-sur-Yvette, France

Structure of human collagen fiber organization in connective tissues

N. Morel*, M. Le Strat†, E.Budyn◇

Department of Mechanical Engineering
Ecole Normale Supérieure Paris-Saclay, University Paris-Saclay
*e-mail: nathan.morel@ens-paris-saclay.fr
† e-mail: maxime.le_strat@ens-paris-saclay.fr
◇ e-mail: elisa.budyn@ens-paris-saclay.fr

KEYWORDS: Cortical bone; Osteocyte; Collagen fiber; Composite; Mechanical constitutive law.

ABSTRACT

Introduction

Bone is known to be a mechanostat and adapt its microstructure to the loading it is subjected to. With aging and certain pathologies this adaptation is modified [5]. As a baseline, we propose to identify in healthy bone, the limit of elasticity of the constitutive behaviors of the materials phases present in the micro-environment of an osteocyte.

Materials and Methods

A Representative Volume Element, RVE, of the bone matrix around an osteocyte process was constructed by segmentation of fluorescent confocal microscopy observations [5] of the cell and Transmission Electron Microscopy (TEM) images of the mineralized fibers [2]. The mineralized collagen fibers of the extracellular matrix around the osteocyte cytoplasmic extension was modeled by 3D helicoidal tubular structures parameterized by the TEM measurements. Only dark osteons of which the collagen fibers display a 60°/120° orientation were considered [2]. These osteons usually form in regions that mostly work under tension [1]. Because long bones such as tibia and femur work under flexion, therefore under compression and tension, both types of loading were modeled at the limit strain of homeostasis: 1.5 micro-strain under compression and 1 micro-strain under tension [3]. As a preliminary approximation, all the materials phases including the hydroxyapatite (HAP), Type I collagen, the proteoglycan interphase, the peri-cellular matrix (PCM), and the cell process were considered linear elastic. The finite element model was implemented in Abaqus. The obtained principal components of the stress fields of the different phases were projected on a unit sphere to identify directional behaviors and limits of elasticity.

Results and discussions

Under 1.5 compressive micro-strain of the RVE, the hydroxyapatite phase displays significantly higher compressive stress values than other phases. The cell process is under a minimal principal stress of -5 to -45 Pa compression and a maximum principal stress in mixed mode of 2 Pa tension and 10 Pa compression.

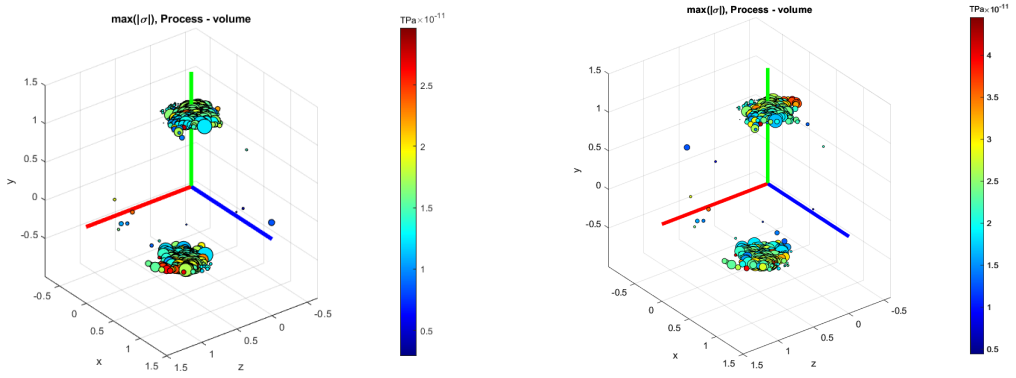

(a) Tension (b) Compression

Figure 1: Representation of the maximum of the absolut value of stress and its direction

Under 1 tensile micro-strain of the RVE, the hydroxyapatite phase displays tensile stress values higher than other phases but most of the phases are under tension with an homogeneous distribution. The cell process is under a minimal principal stress of -25 Pa to 10 Pa compression and a maximum principal stress in mixed mode of 30 Pa tension and 7 Pa compression.

Our model showed in the RVE under $1\mu\epsilon$ tension, the maximum tensile stress values in the HAP corresponds to the damage threshold at the nanos-cale identified by an dual experimental-numerical approach [4]. Moreover, the model showed that fiber orientation generate a stress distribution that is more adequate to either tensile or compressive loading.

REFERENCES

[1] J. Skedros, K. E. Keenan, T. J. Williams, C. J. Kiser, Secondary osteon size and collagen/lamellar organization ("osteon morphotypes") are not coupled, but potentially adapt independently for local strain mode or magnitude, J. Struct. Biol. **Vol**:181 95-107, 2013

[2] N. Reznikov, R. Shahar, S. Weiner, Three-dimensional structure of human lamellar bone: The presence of two different materials and new insights into the hierarchical organization, Bone. **Vol**:59, 2014

[3] R. Al Nazer, J. Lanovaz, C. Kawalilak, J.D. Johnston, S. Kontulainen. Direct in vivo strain measurements in human bone—A systematic literature review. *Journal of Biomechanics* **Vol**:45 27-40, 2011.

[4] J. Jonvaux, T. Hoc, É. Budyn. Analysis of micro fracture in human Haversian cortical bone under compression. *Int. J. Numer. Meth. Biomed. Engng.* **Vol**:28 974-998, September 2012.

[5] E. Budyn. A Bone-on-Chip as a 3D in Vitro Platform to assess the Effect of Stem Cell Age on Tissue Quality and Test Medicines. *Tissue Engineering: Parts A, B, and C.* **Vol**:29 13-14, 2023.

Identification of process parameters in PBF-LB additive manufacturing taking into account machine behavior

L. CHAFFARD – H. ROSSO – K. GODINEAU

TER M1 2023-2024

FINAL DEFENCE OF RESEARCH PROJECTS

April 2, 2024, Gif-sur-Yvette, France

école normale supérieure paris–saclay

TER M1 2023-2024
FINAL DEFENCE OF RESEARCH PROJECTS
April 2, 2024, Gif-sur-Yvette, France

Identification of process parameters in PBF-LB additive manufacturing taking into account machine behavior

L. Chaffard[a], H. Rosso[b], K. Godineau[c]

Mechanical Engineering Department
École normale supérieure Paris-Saclay
4 Avenue des Sciences, 91190 Gif-sur-Yvette, France

[a] e-mail: lohan.chaffard@ens-paris-saclay.fr, [b] e-mail: hugo.rosso@ens-paris-saclay.fr,
[c] e-mail: kevin.godineau@ens-paris-saclay.fr

KEYWORDS: Additive manufacturing; Powder Bed Fusion - Laser Beam (PBF-LB); Skywriting; Influence of trajectory parameters.

ABSTRACT

General Context

In metal additive manufacturing by laser powder bed fusion, the geometry and mechanical characteristics of the produced parts are both generated during the manufacturing process. The laser path and the energy applied to the powder determines the quality of the part. To master trajectories and energy, studies demonstrate the importance of controlling power and velocity [1]. However, treatments performed by numerical control of the machine result in slowdowns and deviations of the effective trajectory which impact energy applied and thus the integrity of the part [2]. There are many parameters other than speed and power that can be used to modulate energy input locally. Yet, few studies have focused on the influence of these parameters [3]. Our study focuses on 3 parameters which involved in the numerical control to change the requested trajectory into a new one for the actuators. The parameters are: the **delays between trajectory segments**, the **skywritting (addition of small trajectories)**, and the **delays in laser ignition and extinction**. The goal of this study is to understand the impact of these parameters to improve a knowledge model of the PBF-LB machine.

Identification methods

In order to observe the influence of these parameters, various trajectories have been developted and executed on a test bench and then on a PBF-LB machine. These tests consisted of engraving plates and acquiring the real-time laser position at 100kHz. Different experimental plans were designed and implemented for each parameter. The differences between the command and the effective trajectory have been observed, which allowed to improve the behavior models for each of the three parameters.

Results

The results show that the trajectory sent to the actuators is the consequence of a filtering of the CAM trajectory. This is an interpolation solution that limits the solicitations of

the actuators. The parameter **'delays between segments'** affects the command before filtering to make the filtered trajectory closer to the initial one (cf. Fig. 1 (b)). However, this leads to a local decrease in speed, so power must be modulated to remain at constant energy. The second parameters called **skywrrinting** allow local modification to ensure that the laser pass exactly on the CAM trajectory (cf. Fig. 1 (c)). The **delays in laser ignition and extinction** allow control of the beginning or end of material fusion. It could be use to ensure that the laser stop melting the metal at the right location when adding trajectories is used.

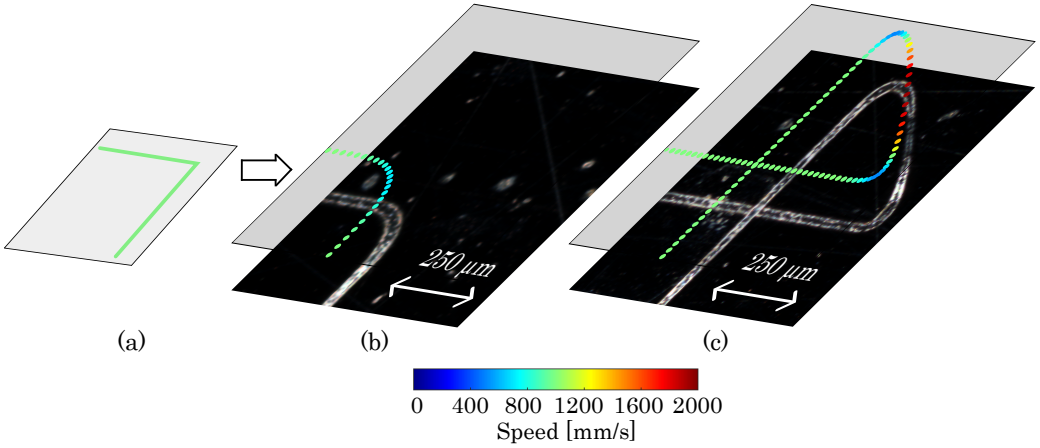

Figure 1: Influence of parameters on the effective trajectory; CAM requested trajectory (a), trajectory with delays (b), trajectory with adding trajectories (c)

In conclusion, the established behavior models in a digital numerical simulator of the PBF-LB machine have been improved. This simulator allows to predict the machine's behavior during the execution of a trajectory. The Fig. 1 shows two engravings from the same CAM trajectory and the associated simulation (cf Fig. 1 (a)) but with different parameters. The work carried out in this TER will enable the development of an automatic method. This method will determine, based on kinematic, geometric, and energetic criteria, an optimal recipe of parameters. It will be optimized to achieve an effective trajectory starting from a known velocity-power couple.

REFERENCES

[1] J.P. Oliviera, A.D. LaLonde, J. Ma. *Processing parameters in laser powder bed fusion metal additive manufacturing.* Materials and Design, 2020.

[2] M. Carraturo, B. Lane, H. Yeung, S. Kollmannsberger, A. Reali, F. Auricchio *Numerical Evaluation of Advanced Laser Control trategies Influence on Residual Stresses for Laser Powder Bed Fusion Systems.* Integrating Materials and Manufacturing Innovation, 2020.

[3] H. Yeung, B.M. Lane, M.A. Donmez, J.C Fox, J. Neira *Implementation of Advanced Laser Control Strategies for Powder Bed Fusion Systems.* Additive Manufacturing, 2018.

Development of a user element generator for Abaqus™ from Matlab™

T. JANNIN – M. SANVOISIN – P-A GUIDAULT

TER M1 2023-2024

FINAL DEFENCE OF RESEARCH PROJECTS

April 2, 2024, Gif-sur-Yvette, France

école normale supérieure paris–saclay

TER M1 2023-2024
FINAL DEFENCE OF RESEARCH PROJECTS
April 2, 2024, Gif-sur-Yvette, France

Development of a user element generator for Abaqus^{TM} from Matlab^{TM}

T. Jannin*, M. Sanvoisin*, P.-A. Guidault◇

*Département Génie Mécanique, École Normale Supérieure Paris-Saclay
4 Avenue des sciences, 91190, Gif-sur-Yvette, France.
e-mail: {thomas.jannin, maceo.sanvoisin}@ens-paris-saclay.fr

◇ Université Paris-Saclay, CentraleSupélec, ENS Paris-Saclay
CNRS, LMPS - Laboratoire de Mécanique Paris-Saclay
91190, Gif-sur-Yvette, France.
e-mail: pierre-alain.guidault@ens-paris-saclay.fr

KEYWORDS: Abaqus^{TM} ; Matlab^{TM} ; User Element

ABSTRACT

General Information

Many finite element solvers offer engineers the ability to develop user-defined elements. In order to use elements with specific behaviours, non-linearities, equivalent models, for example [1]. These elements are often developed in C or FORTRAN. To make the development of user elements simpler, there is a need to develop a tool that can be used to code complex models through an interpreted language such as Matlab^{TM}. Such a tool has been developed at LMPS for user materials, but does not exist for user elements. The aim of this study is to develop a Matlab^{TM} code package that can be used to both develop, debug and generate a user element for Abaqus^{TM}.

1 Methods

The method consists in the generation of a C code via Matlab^{TM} function *codegen*. The user element behaviour is implemented in a *.m* function which has the same arguments and output that a User ELement (UEL) subroutine in Abaqus^{TM} [2]. That function can be debugged with a Matlab^{TM} Newton-Raphson solver before being generated in C - in a package that contains all the headers needed for C code - with *codegen*. The generated code can be compilated by Abaqus 6.21-6 with *g++ 12.2.0* compiler for example. The User Element can write informations in the *.log* file or in a new *.txt* file created in the folder where the job is executed.

2 Results

To test our methods, we developed a user element described by the rheological model of the **Figure** 2a [3]. Node 2 is subjected to a load $\mathbf{F} = F\mathbf{e_1}$ where F describes the following cycle : [0 ; 1800 N ; -1800 N ; 1980 N ; -1980 N ; 0]. We were able to validate the method used to generate the user element for a 1D element with a comparison by superimposing the Matlab^{TM} simulation and the Abaqus^{TM} calculus results on **Figure** 2b.

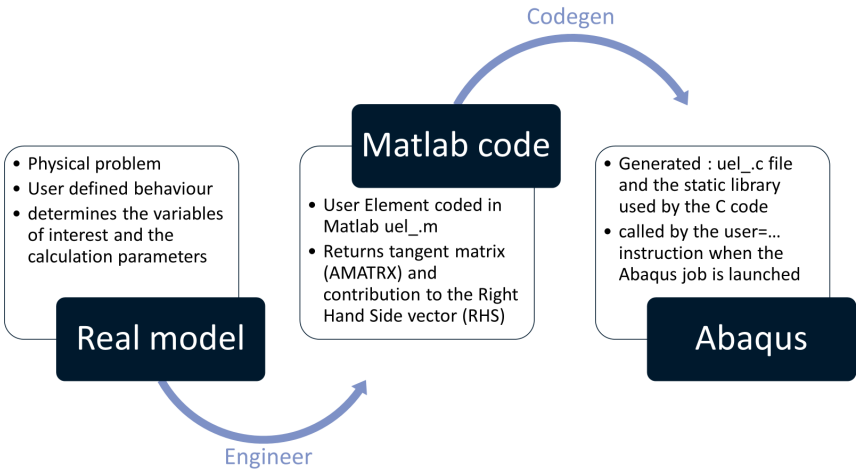

Figure 1: Illustration of the method of developement of the user element

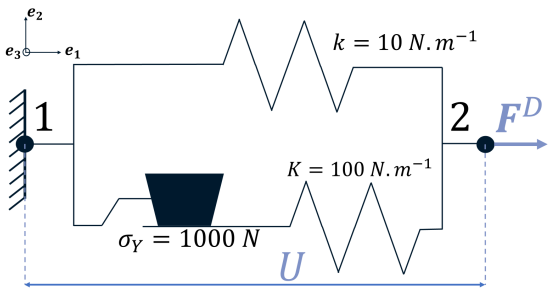

(a) Rheological model

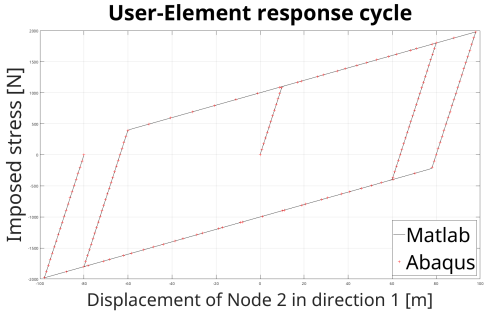

(b) Matlab and Abaqus results superimposed

3 Conclusion and future work

Our work can be developed further with the generation of 3D models and other behaviours than plasticity. It can include for example beam models or plasticity with hardening. It could be interesting to develop sliding models in analogy with plasticity models.
Further work can also include development of Matlab tools that can operate on Abaqus^{TM} *.log* or *.txt* generated file to debug or post-process directly in Matlab^{TM}.

REFERENCES

[1] Richard Verwaerde, Pierre-Alain Guidault, and Pierre-Alain Boucard. A non-linear finite element connector model with friction and plasticity for the simulation of bolted assemblies. *Finite Elements in Analysis and Design*, 195:103586, 2021.

[2] Dassault System Simulia Corporation. *Abaqus/Standard User Subroutines*, 2021.

[3] Marc Bonnet and A. Frangi. *Analyse des solides déformables par la méthode des éléments finis*. Editions de l'Ecole Polytechnique, 2006.

Detecting layering defects on the LPBF process using computer vision methods

A. SAINTY – V. ROY – Y. QUINSAT

TER M1 2023-2024

FINAL DEFENCE OF RESEARCH PROJECTS

April 2, 2024, Gif-sur-Yvette, France

école normale supérieure paris—saclay

TER M1 2023-2024
FINAL DEFENCE OF RESEARCH PROJECTS
April 2, 2024, Gif-sur-Yvette, France

Detecting layering defects on the LPBF process using computer vision methods.

Armand Sainty*, Valentine Roy*, Yann Quinsat*

* Mechanical engineering department
Ecole Normale Supérieure Paris Saclay
4 Avenue des Sciences, 91190 Gif-sur-Yvette
email : armand.sainty@ens-paris-saclay.fr
email : valentine.roy@ens-paris-saclay.fr

KEYWORDS: Additive Manufacturing; Laser Powderbed Fusion; Computer Vision.

ABSTRACT

General context

The LPBF process works by spreading a thin layer of a fine metal powder. The powder is then fused by a high power laser. This cycle is repeated for every layer of the part. The powder is spread by a recoater : a cylinder spinning in the opposite direction of its motion, pushing a bead of powder. At this stage, defects such as recoater hopping, streaking and incomplete spreading can occur. The causes of these defects are multiple and ill understood. Being able to automatically detect these will help to better understand the defects and link them to process parameters. As of yet, it isn't possible to automatically detect these defects with sufficient accuracy without using very high resolution imagery [2]. Approaches using the integrated camera of the machine and classification networks have been tested, but yield unreliable results [3, 4].

Methods

This project sets out to identify automatically the defects present on the printbed after every layering phase in order to obtain a part health, layer by layer as seen of figure 1. The knowledge from the manufacturing report of the part will be useful to link the layering defects and the mechanical properties of the produced parts. This project was carried out using the photographs provided by the integrated camera on a AddUp 300 LPBF machine. This camera has a resolution of about 0.32 mm/pixel. A large database containing close to 25000 pictures, Was provided to us in 200x200 pixel tiles, as well as 25x25 pixel tiles was provided [4]. The tiles are labeled "OK", "recoater hopping", "streaking" and "incomplete spreading". Previous work using this database consisted in training and comparing several neural network architectures to classify the patches. The accuracy of these neural networks peaked at about 65%. This is due to the fact that the database is very unbalanced as most patches were labeled as "OK" and only very little were labeled with defects (figure 2). A specializing a pre-trained network could yield better results, but the network sizes must be identical. Some types of networks can be pre-trained and can yield very high accuracy results using very high resolution images (6 µm/pixel).[2] However, using another type of neural networks has been suggested. Segmentation models are capable of generating masks on images, in order to decompose the image in the elements that constitute it. Specializing a pre-trained network could prove effective to segment defects from the powder bed. For this project the Segment Anything Model (SAM) [1] from Meta AI was chosen as it is

trained on a very large database. It shows excellent capabilities in generalizing (being able to segment an object that it has not been trained on). Early trials show that it is fairly capable at detecting melted areas on the powderbed, but failed to mark smaller defects. The pictures from the database have very uneven lighting due to the presence of the recoater. An image correction program has been developed in order to make the lighting more homogeneous. This will hopefully increase the performance of the model.

Key results

Specializing SAM on the detection of dark grey elements on a light gray background is a promising lead. By training SAM to detect melted areas on the post melting images, it is reasonable to believe that SAM will be able to detect defects (that are generally darker) on the post layering pictures. Indeed, the ideal post layering picture is perfectly homogenous. Any non-homogenous patch is therefore an anomaly and a likely defect. SAM would hence be able to provide the location of anomalous patches, which can then be processed by a classification algorithm. The main benefit is that this would greatly reduce the number of "OK" patches analysed, meaning the classification model will only have to determine the type of anomaly, and not determine whether it is an anomaly or not.

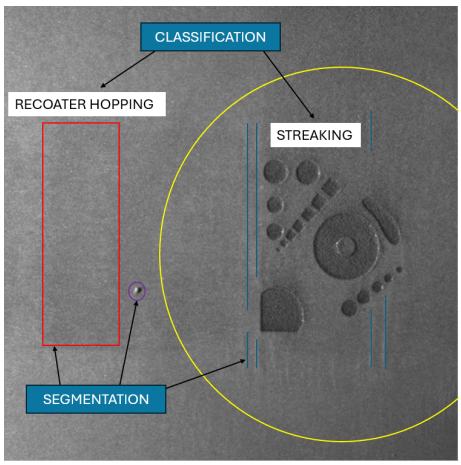

Figure 1: Desired program output

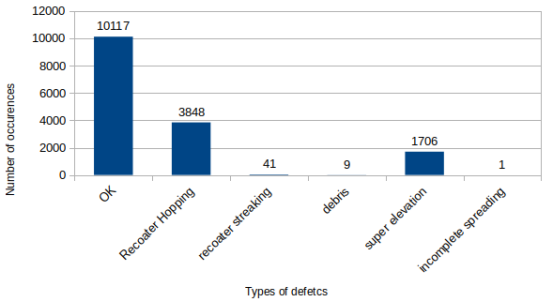

Figure 2: Number of images in each class

References

[1] Alexander Kirillov et al. Segment anything, 2023.

[2] Fischer et al. Monitoring of the powder bed quality in metal additive manufacturing using deep transfer learning. *Mater. Des.*, 222(111029):111029, October 2022.

[3] Luke Scime et al. Layer-wise anomaly detection and classification for powder bed additive manufacturing processes. *Additive Manufacturing*, 36:101453, December 2020.

[4] Thomas Rey. Analyse des défauts de mise en couche et de lasage pour le procédé lpbf. *Ecole Normale Supérieure Paris-Saclay*, 2023.

Modeling the behavior of woven fabrics subjected to knife stabs

B. P. TEXIER – N. IDERNE – C. HA-MINH

TER M1 2023-2024

FINAL DEFENCE OF RESEARCH PROJECTS

April 2, 2024, Gif-sur-Yvette, France

école normale supérieure paris–saclay

TER M1 2023-2024
FINAL DEFENCE OF RESEARCH PROJECTS
April 2, 2024, Gif-sur-Yvette, France

Modeling the behavior of woven fabrics subjected to knife stabs

Pauline Texier*, Nathan Iderne*, Cuong Ha-Minh◇

* Département de génie mécanique
École Normale Supérieure, Paris Saclay University
e-mail: pauline.texier@ens-paris-saclay.fr, nathan.iderne@ens-paris-saclay.fr
◇ Laboratoire de mécanique Paris-Saclay
École Normale Supérieure, Paris Saclay University
e-mail: cuong.ha-minh@ens-paris-saclay.fr

KEYWORDS: Fabric behavior; Friction analysis; Impact behavior; Textile composite.

ABSTRACT

General information : This study explores fabric behavior under the impact of a knife by approaching it in various scales: macroscopic, mesoscopic and microscopic. Traditional models often overlook this perspective, motivating an investigation into the macroscopic behavior of fabric under dynamic conditions. The primary aim of this research is to understand how fabric behaves when a knife stabs it, specifically focusing on energy dynamics and the impact of friction forces.

Methods : The current understanding of fabric behavior is only theoretical for now, and lacks an experimental approach. This study aims to fill this gap in knowledge by employing a simulated and finite element perspective and using MatLab and LS-Dyna for enhanced interpretability. MatLab is used to implement the theoretical equations of the theoretical model. An initial velocity is imposed on the projectile and the impact causes various deflections on the fabric.

Results : First, the theoretical model implemented (Figure 1.a) needs to fit the experimental results found by previous research [3]. Without considering friction, the macroscopic model demonstrates a constant total energy, which is accurate to a frictionless model (Figure 1.b). The introduction of an initial velocity reveals dynamic changes in projectile speed, particularly notable upon fabric perforation. The study explores fabric pyramid and projectile displacements, emphasizing the influence of friction forces. Indeed, the introduction of friction forces generates an energy loss that changes according to the knife's geometry (Figure 1.d). For the cone studied (Figure 1.c) the friction energy is:
$\Delta E_{fri} = 2\pi e\, r\, V_i\, dt\, (-s \sin(90 - \alpha) m_p a)$.
LS-DYNA is used to create a digital twin of the macroscopic model, to avoid conducting an expensive test, which needs a high-speed camera, to compare the analytical model with real experiments. In the following, the analytical model will be compared with the numerical model to lead the needed experiments in a quick and efficient manner.

Conclusions : This research contributes to a deeper understanding of fabric behavior under dynamic conditions, highlighting the significance of treating fabric as a plate. The observed energy dynamics and frictional effects offer valuable insights into fabric deformation. Further studies could explore the

application of this new perspective to different materials and dynamic scenarios. Investigating the potential practical implications of these findings in real-world applications is recommended.

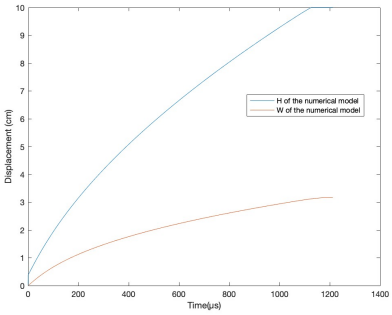

Theoretical displacement of the fabric pyramid [1] for an initial velocity of 375 m/s

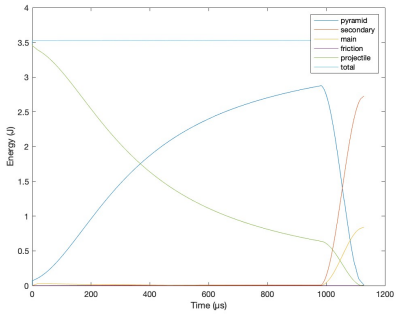

Evolution of the energy in the system for an initial velocity of 50 m/s

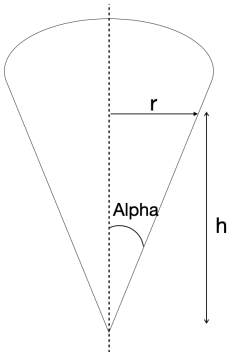

Geometry of an cone-shaped knife

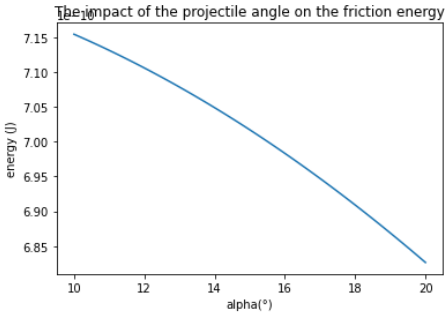

Evolution of the friction energy and the knife's geometry

Figure 1: Results obtained with the MatLab model

REFERENCES

[1] Tuan Long Chu, Cuong Ha-Minh, Abdelatif Imad, Quoc Hoan Pham. *Towards an efficient multi-scale numerical model of the impact behavior of woven materials with Global/Local approach.*

[2] Julie E. Samuels. *Stab Resistance of Personal Body Armor -NIJ Standard–0115.00.* U.S National Institute of Justice.

[3] Cuong Ha-Minh, Abdellatif Imad, François Boussu, Toufik Kanit. On analytical modelling to predict of the ballistic impact behaviour of textile multilayer woven fabric. *Composite Structures*

[4] Smith JC, McCrackin FL, Scniefer. Stress–strain relationships in yarns subjected to rapid impact loading. *Journal of Research of the National Bureau of Standards* **Vol 5**:288-302